Available online at www.sciencedirect.com
ScienceDirect
Journal of Sound and Vibration 318 (2008) 1050–1076
JOURNAL OF SOUND AND VIBRATION
www.elsevier.com/locate/jsvi

Acoustic based sensing of orthogonal radiating functions for three-dimensional noise sources: Background and experiments

Simon G. Hill[a,*], Scott D. Snyder[b], Nobuo Tanaka[a]

[a]*Department of Aerospace Engineering, Tokyo Metropolitan University, 6-6 Asahigaoka, Hino-shi, Tokyo 191-0065, Japan*
[b]*Business and Administration, Charles Darwin University, Darwin, Northern Territory 0909, Australia*

Received 28 July 2006; received in revised form 18 April 2008; accepted 22 April 2008
Handling Editor: C.L. Morfey
Available online 11 June 2008

Abstract

This paper is concerned with the development of global, orthogonal, radiation patterns for 3D noise sources. Traditionally, sensing strategies for the active control of such sources is postulated on a vibration pattern and a set of radiation transfer functions. However, in practice not all noise sources are vibrational and accurate radiation functions (which may or may not be time invariant) are difficult to measure beyond the laboratory. The orthogonal basis functions developed in this work are based on a set of acoustic monopoles (arranged in a 3D array) described as multipoles, to decompose an independent set of radiating functions. The aim of the work is the design of practical acoustic sensing systems amendable to active noise control of large, complex, noise sources, or simply the characterisation and quantification of global radiation from such sources. Through experiments on a non-structural, 3D noise source, we examine the feasibility of the developed approach and compare and contrast the estimate of radiated power based on 2D and structural centric approaches.

1. Introduction

The characterisation, control or minimisation of noise radiation from 3D noise sources into free or semi-free spaces is a problem faced regularly by engineers in a wide range of practical situations. The problem has been tackled heavily from a theoretical modelling point of view [1–5], but also with active [6,7] and passive [8,9] noise control techniques. However, in the area of active control the majority of the work has tended to focus on structural, 1D and 2D sources, leaving the 3D field almost untouched. This point was noted by Cunefare [10] back in 1991, and in the proceeding years few breakthroughs in the area of sensing global quantities for large, free field sources have been achieved.

While it appears possible to apply some 2D sensing strategies to 3D bodies, the fundamental pretence is still a structural, 2D noise problem. There are, however, many free space noise sources of practical interest that are not completely, or sometimes even partially, structural. It is then not a straightforward process to apply

*Corresponding author. Tel./fax: +81 42 585 8623.
E-mail address: sghill@sd.tmu.ac.jp (S.G. Hill).

0022-460X/$ - see front matter © 2008 Elsevier Ltd. All rights reserved.
doi:10.1016/j.jsv.2008.04.044

previous methodologies for global error sensing in these cases. This work then makes a novel contribution to the design of sensing systems for active control (of 3D sources), acoustic modelling methods and source characterisation techniques.

The classical, large, 3D noise radiation problem, which has received much attention, is that of electrical transformer radiation. It has long been recognised that the source of the noise is the magnetostrictive forces within the transformer (laminated) core [11–13]. However, manufacturers have been unable to reduce noise emissions. One of the early applications of active noise control to a large 3D noise source was a 15,000 KVA electrical transformer, carried out by Conover [12]. His pioneering work illustrated significant problems which face all active noise control systems. Using sound pressure measured at a single point in the far field as an error signal, Conover was able to attenuate radiating noise from the electrical transformer. However, attenuation was localised around the position of the error sensor and increases in the sound pressure level at other points around the transformer were measured. Hesselmann, Angevine and colleagues [14–16] reported that global control could be achieved for a transformer in an anechoic room provided that the transformer was completely surrounded by loudspeakers. The practical and economical extension of this result to existing substation installations has so far been difficult. Angevine and colleagues [16] also concluded that the attenuation was dependent on the number of control sources and that this dependence was stronger at lower frequencies, a result also reported by Li and colleagues [17,18] for a transformer in the field.

The work on large electrical transformers illustrates the *need* for a global rather than a local error criterion and also the *need* for a large number of error sensors to measure the chosen criterion. For an industrial sized transformer (typically in the size range of $5\,\mathrm{m} \times 5\,\mathrm{m} \times 5\,\mathrm{m}$), a significant number of microphones (placed with a separation of less than $\frac{\lambda}{2}$) would be required to surround the structure to obtain a global error measurement. However, sending all of these signals to a controller will quickly overtax the controller's central processing unit and reduce the performance of the system. To seek to address this problem, researchers have turned to modal filtering [7,19–27]. In modal filtering, many point measurements are reduced to a smaller number of estimates of global quantities, traditionally structural modes of vibration. It is then the aim of the control system to minimise the resulting few filtered signals, rather than the signals from all of the point sensors.

There have been many orthogonal functions used to describe acoustic power [28–41]. In all these developments, which are all structural based and limited to 1D or 2D sources, the goal has been to write the radiation as the sum of vibrational patterns which contribute orthogonally to the global error: radiated power. Typically only the first few vibration patterns need to be considered to give an accurate estimate of the criterion at low frequencies.

Other work that has focused on 3D sources includes Cunefare et al. [42], where they examined the radiation modes of a rectangular box based on the mapped spherical harmonics of a sphere placed in the centre of the box. The spherical harmonics were compared to a BEM analysis of the radiation modes. The orthogonal patterns (based on the spherical harmonics of a sphere) were not based on any structural information; however, practical measurement of the patterns is problematic and the frequency dependence of the patterns was not examined. In a similar vein there is a body of work in which the radiation of 3D sources is modelled by multipoles of pulsating spheres [3,5,28,43,44]. In a group of solely theoretical work by Cunefare and Koopmann [10,45,46], a rectangular box is examined though a BEM analysis. The box has a simply supported panel on the top. Based on assumed velocity amplitude of the panel structural modes, optimal amplitude and phase characteristics for a set of control sources (placed on the box surface) were evaluated with respect to a quadratic expression of total radiated pressure. Almost 20 dB reduction was achieved. Later Giordano and colleagues [6], used the noise control method by Cunefare and Koopmann [10,45,46] in simulation to examine the control of sound power from a 3D box. The surface velocity on the 3D box was measured in experiments. This data formed a basis for a theoretical study in which four speakers were placed on the top of the panel (in each corner) of the box. In the control strategy, a BEM analysis was used to optimise the amplitude and phase of each speaker to minimise total radiation with respect to radiated power. The calculated reduction of radiated power from the 3D source was 10 dB.

It appears from literature that state of the art sensing strategies for 3D noise sources postulates a vibration based source and that vibration data which accurately relate to a global error are readily available. Yet it also appears that there are few works which are concerned with practical measurements of the orthogonal radiation patterns for non-structural 3D noise sources.

In this article we focus on the practicalities of obtaining a global error signal for large 3D noise sources (where a large number of sensors *are* required), be they structural or non-structural. To date much research in the area of active control has illustrated the difficulties in moving from a 2D to 3D problem. There are several limitations which such an approach faces:

- The dimension of the system (a large number of control inputs/outputs and number of sensors are required for an accurate global error and adequate control authority);
- The limited applicability of 2D techniques; and
- The structural centricity of many approaches (assuming the availability of vibration data which relates *accurately* to radiated pressure).

This paper has a sensing focus; however, should active control be attempted, the achievable attenuation will be dependent upon a hierarchy for factors, the most important being the number, type and location of the secondary actuators [47–49]. The novel contribution of this work is two-fold. Firstly, we develop 3D orthogonal functions with respect to radiated sound power, with no restriction to structurally based sources. The strategy can then be applied to any source: structural or non-structural. At the heart of the process is the development or orthogonal contributors to radiated power based on phased (+1 or −1) combinations of a 3D array of monopoles. The second contribution is an experimental investigation on a non-structural, 3D noise source. In experiments we compare two, 2D sensing approaches to the novel 3D decomposition of radiated power from the source. We demonstrate through experiments the sensing strategy and also data fusion hardware capable of filtering 128 signals in real time at 5 kHz.

2. Quadratic performance development

Consider a 3D noise source on an infinite baffle. To measure global radiation from the source in the acoustic domain, sensors need to be placed all around the source. However, as the geometric size of the source increases the number of required sensors will significantly increase. The approach would then quickly become impractical as a controller cannot, quickly and robustly, converge to give a global radiation reduction for a rapidly increasing number of error signals. As mentioned in the previous section, in an attempt to reduce the number of signals a controller has to analyse and minimise, researchers have turned to modal filtering and data fusion methods. In the work here, at the heart of the developed 3D sensing strategy is a modal filtering/data fusion process.

Consider an acoustic sensing system of the form illustrated in Fig. 1. In the process of developing this type of sensing system where a relatively large number of measurements are condensed into a smaller number of error signals before being input to the controller, it is desirable to be able to state the global performance measure, J, as a quadratic function,

$$J(t) = \mathbf{q}^{\mathrm{T}}(t)\mathbf{A}(\omega)\mathbf{q}(t) \tag{1}$$

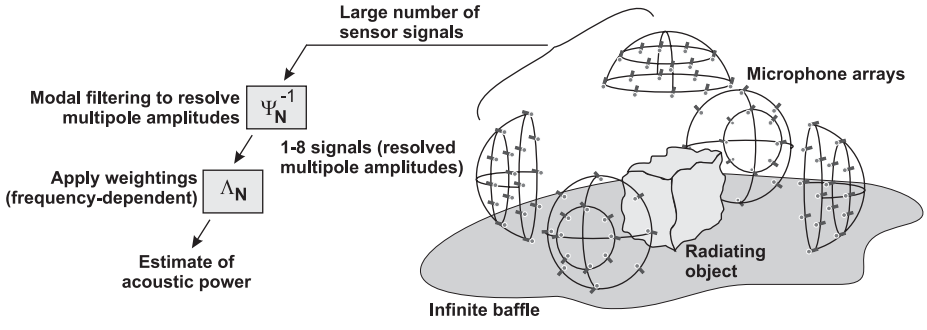

Fig. 1. General acoustic sensing system for a 3D noise source.

In Eq. (1), **q** is a vector of quantities to be measured (essentially system states that are time dependent) and **A** is a square weighting matrix which is typically frequency dependent. As a simple example, if the global performance measure is energy in a vibrating structure, the terms in **q** could be modal displacements and velocities. The terms in **A**, would then be modal masses and stiffnesses such that the global performance measure is the sum of modal kinetic and potential energies. The dependent variables in Eq. (1) have been chosen to reflect the procedure used in the experiments, where a large number of sound pressure signals are filtered (using only multiplication and addition) in the time-domain; the result is then a set of system states (**q**) which are time dependent. The weights used in the filtering process are dependent on the values in **A**, which is frequency dependent. However, for application in the time-domain, the weights must be selected a *single* frequency, thus reducing the filtering process to simply multiplication and addition. Stated differently, the modal filtering procedure is performed on the real-time pressure signals, the outputs of which (**q**) are then Fourier-transformed to evaluate the cost functional at each frequency.

Stating the global performance measure as a quadratic function offers a number of obvious benefits to the system designer, regardless of the control approach used. The frequency dependent weighting factors (in **A**) can be used to guide problem truncation, as well as being necessary for either frequency weighted LQG design [50–52] or any design using a $\mathscr{H}_\infty$ or $\mathscr{H}_2$ error criterion. If adaptive feedforward control is being used, as is common in active noise control, then **A** must be diagonal to be of maximum benefit. The quantities in **q** can then be measured as error signals, and passed through filters with frequency characteristics defined by the diagonal terms in **A** prior to being used by the adaptive algorithm [36].

The aim of the following theoretical development is the derivation of a quadratic expression for radiated acoustic power in terms of some fundamental 3D, "mode-like" quantity. This expression will provide the starting point for development of the modal filtering sensing strategy that is the ultimate target of this work.

As mentioned in the literature review the problem with previous modal filtering approaches, used to develop sensing strategies for active noise control, is that they assume that the sound source *is* a radiating structure and may require knowledge of the structural mode shape functions. Certainly a large number of free space noise problems arise from structural acoustical radiation, but not all. Furthermore, it is unrealistic to assume that accurate knowledge of the mode shape functions of practical structures can always be obtained; consider the problem of radiation from a electrical transformer (of any size). In the formulation here, it will be assumed that the sound source is planar and radiating into a half-space. This assumption could be removed and the problem reformulated for radiation into some other space (for example, an enclosed space) without a great deal of difficulty. What will be avoided is a formulation based upon structural mode shape functions.

Consider Fig. 1 where a planar sound source is situated in an infinite baffle subject to harmonic excitation and radiating in air with a coordinate system defined in Fig. 2. The acoustic power W radiated by this source can be evaluated by integrating the far-field acoustic intensity over a hemisphere enclosing the source and can be written as

$$W = \int_0^{2\pi} \int_0^{\pi/2} \frac{|p(\mathbf{r})|^2}{2\rho_0 c_0} |\mathbf{r}|^2 \sin\theta \, \mathrm{d}\theta \, \mathrm{d}\phi \tag{2}$$

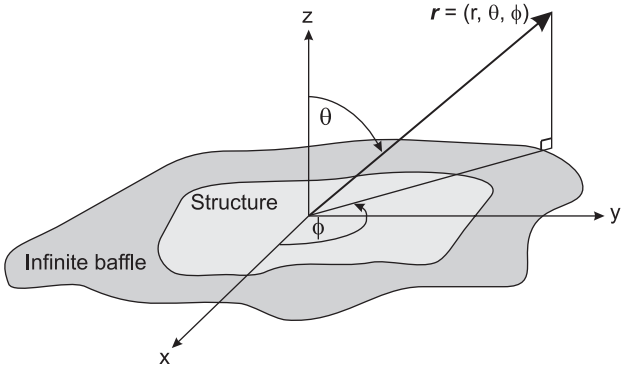

Fig. 2. System geometry.

In Eq. (2), $p(\mathbf{r})$ is the acoustic pressure at some location, $\mathbf{r}$ in space, with the location defined by the spherical coordinates $\mathbf{r} = (r, \theta, \phi)$. The terms ρ_0 and c_0 are the density of air and speed of sound in air, respectively.

2.1. The 3D decomposition approach

For the development here, let the total acoustic pressure, $p(\mathbf{r})$, be decomposed in terms of acoustic multipole radiation patterns, in a similar fashion to the 2D approach in Ref. [25]; analogous to the decomposition of a structural velocity distribution in terms of *in vacuo* mode shape functions. Sound pressure is therefore described as

$$p(\boldsymbol{r}) = \sum_{i=1}^{\infty} a_i \psi_i(\boldsymbol{r}) \tag{3}$$

where a_i is the amplitude of the ith multipole, and $\psi_i(\boldsymbol{r})$ is the radiation transfer function for the ith multipole between the origin and the location $\boldsymbol{r}$ (i.e., the value of the radiation pattern generated by the multipole at location $\boldsymbol{r}$ in space). The multipole radiation patterns used in the decomposition will be derived from in-phase/out-of-phase combinations of "virtual" monopoles situated in an array above the baffle surface, as illustrated in Fig. 3. The multipole approach can easily allow for the inclusion of more "virtual" monopoles in the modelling process which in turn increases the accuracy of the estimate along with its bandwidth, as will be shown later in this article. Eq. (3) presents the idea that the total sound radiation (from any source) can be written in terms of a sum of orthogonal multipole [25] radiation patterns. Then the total radiation from any noise source can be categorised (and measured) in terms of the individual orthogonal multipole radiation patterns.

Truncating Eq. (3) to n acoustic multipoles enables the pressure to be written in matrix form

$$p(\boldsymbol{r}) = \boldsymbol{\psi}(\boldsymbol{r})\boldsymbol{a} \tag{4}$$

where the parameter $\boldsymbol{a}$ is a column vector with the complex amplitudes of the n multipoles under consideration and $\boldsymbol{\psi}(\boldsymbol{r})$ is a row vector with elements corresponding to the values of the radiation transfer functions for the n multipoles included in the calculation. The theoretical contribution of this work is the development of orthogonal basis functions, $\boldsymbol{\psi}$, for 3D sources (which can be structural or non-structural). Later, we present an experimental example which in essence entails measuring each of the multipole amplitudes, $\boldsymbol{a}$, in a practical setting.

Using Eq. (2) to expand the pressure term in Eq. (4), sound power can be expressed as

$$W \approx \int_0^{2\pi} \int_0^{\pi/2} \frac{\boldsymbol{a}^{\mathrm{H}} \boldsymbol{\psi}^{\mathrm{H}}(\boldsymbol{r}) \boldsymbol{\psi}(\boldsymbol{r}) \boldsymbol{a}}{2\rho_0 c_0} |\boldsymbol{r}|^2 \sin\theta \, \mathrm{d}\theta \, \mathrm{d}\phi \tag{5}$$

or

$$W \approx \boldsymbol{a}^{\mathrm{H}} \boldsymbol{A}_a \boldsymbol{a} \tag{6}$$

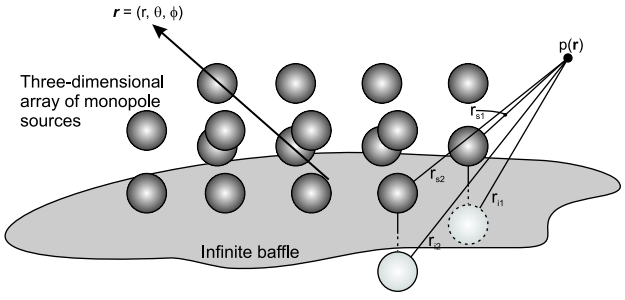

Fig. 3. Monopoles situated above a baffle.

where $\boldsymbol{A}_a$ is a square weighting matrix, the (i,j) term of which is defined by

$$\boldsymbol{A}_a(i,j) = \int_0^{2\pi} \int_0^{\pi/2} \frac{\psi_i^*(\boldsymbol{r})\psi_j(\boldsymbol{r})}{2\rho_0 c_0} |\boldsymbol{r}|^2 \sin\theta \, \mathrm{d}\theta \, \mathrm{d}\phi \tag{7}$$

where ψ is the radiation transfer function between the acoustic multipole volume velocity and acoustic pressure at a point in space. Eq. (7) is independent of any structure properties and only depends on the transfer functions of the most fundamental acoustic radiator, the monopole. Evaluating Eq. (7) numerically for a 3D monopole array is extremely time consuming and so undesirable. To overcome this an analytical solution for free field monopole radiation, which uses the results of past research [53–59], will be developed.

To derive an analytical solution, it is necessary to examine sound power radiation in the near field. Referring to Eq. (6), the terms in $\mathbf{A}_a$ define the power output of a given multipole arrangement operating in isolation (the diagonal terms) and in the presence of other multipoles (the off-diagonal terms). To derive these terms, consider first the simple problem of monopoles radiating in the presence of a baffle. The total acoustic power output from a pair of monopoles is equal to the sum of the power output from each source. The power output of a single monopole source is given by

$$\tfrac{1}{2}\mathrm{Re}\{q_{s1}p_t^*(\mathbf{r}_{s1})\} \tag{8}$$

where q_{s1} is the volume velocity of the monopole source 1 and $p_t(\mathbf{r}_{s1})$ is the total acoustic pressure at the location $\mathbf{r}_{s1}$ from monopole source 1, with the location defined by the spherical coordinates $\boldsymbol{r} = (r, \theta, \phi)$. Assuming for the moment that two sources are in-phase with the same volume velocity, Eq. (8) can be re-expressed for this case as

$$\boldsymbol{q}\left(\mathrm{Re}\left[\frac{\mathrm{j}\omega\rho}{8\pi}\left\{\frac{\mathrm{e}^{-\mathrm{j}kr_{s1}}}{r_{s1}} + \frac{\mathrm{e}^{-\mathrm{j}kr_{i1}}}{r_{i1}} + \frac{\mathrm{e}^{-\mathrm{j}kr_{s2}}}{r_{s2}} + \frac{\mathrm{e}^{-\mathrm{j}kr_{i2}}}{r_{i2}}\right\}\right]\right)\boldsymbol{q}^* \tag{9}$$

where the notation, r_{i1} etc., is based on Fig. 3. Evaluating Eq. (9) at source 1 gives

$$\boldsymbol{q}\frac{\omega k\rho}{8\pi}[(1 + \mathrm{sinc}(kr_{i1}))\ (\mathrm{sinc}(kr_{s2}) + \mathrm{sinc}(kr_{i2}))]\begin{bmatrix}1\\1\end{bmatrix}\boldsymbol{q}^* \tag{10}$$

where $\boldsymbol{q}$ is the monopole amplitudes, fixed to be equal and both in-phase. It is straightforward to derive a similar expression for the power output in the case where two monopole sources are of the same volume velocity, but out-of-phase:

$$\boldsymbol{q}\frac{\omega k\rho}{8\pi}[(1 + \mathrm{sinc}(kr_{i1}))\ (\mathrm{sinc}(kr_{s2}) + \mathrm{sinc}(kr_{i2}))]\begin{bmatrix}1\\-1\end{bmatrix}\boldsymbol{q}^* \tag{11}$$

It is straightforward to generalise this approach to a 3D monopole array. To generate a given multipole pattern, the amplitudes of all sources being fixed and equal, with the phasing of the sources defined by a Hadamard matrix $\mathbf{H}$, which contains a set of orthogonal functions composed of ± 1 [60,61]. For example, if the multipole array were constructed from eight monopole sources, the multipoles would be governed by the relationship

$$\mathbf{H}\boldsymbol{q} = \begin{bmatrix}
1 & 1 & 1 & 1 & 1 & 1 & 1 & 1\\
1 & 1 & 1 & 1 & -1 & -1 & -1 & -1\\
1 & 1 & -1 & -1 & -1 & -1 & 1 & 1\\
1 & 1 & -1 & -1 & 1 & 1 & -1 & -1\\
1 & -1 & -1 & 1 & -1 & 1 & 1 & -1\\
1 & -1 & 1 & -1 & -1 & 1 & -1 & 1\\
1 & -1 & 1 & -1 & 1 & -1 & 1 & -1\\
1 & -1 & -1 & 1 & 1 & -1 & -1 & 1
\end{bmatrix}\boldsymbol{q} \tag{12}$$

the square weighting matrix $\mathbf{A}_a$ in Eq. (7) for a 3D monopole can be calculated as

$$\mathbf{A}_{a3\mathrm{D}} = \boldsymbol{q}\mathbf{H}^{\mathrm{T}}\mathbf{b}\mathbf{H}\boldsymbol{q}^{*} \tag{13}$$

where $\mathbf{b}$ is

$$\mathbf{b} = \frac{\omega k\rho}{8\pi}\begin{bmatrix} 1+\mathrm{sinc}\,(kr_{i1/1}) & \mathrm{sinc}\,(kr_{s2/1})+\mathrm{sinc}\,(kr_{i2/1}) & \cdots & \mathrm{sinc}\,(kr_{sn/1})+\mathrm{sinc}\,(kr_{in/1}) \\ \mathrm{sinc}\,(kr_{s1/2})+\mathrm{sinc}\,(kr_{i1/2}) & 1+\mathrm{sinc}\,(kr_{i2/2}) & \cdots & \mathrm{sinc}\,(kr_{sn/2})+\mathrm{sinc}\,(kr_{in/2}) \\ \vdots & \vdots & \ddots & \vdots \\ \mathrm{sinc}\,(kr_{s1/n})+\mathrm{sinc}\,(kr_{i1/n}) & \mathrm{sinc}\,(kr_{s2/n})+\mathrm{sinc}\,(kr_{i2/n}) & \cdots & 1+\mathrm{sinc}\,(kr_{in/n}) \end{bmatrix} \tag{14}$$

In Eq. (14), $r_{sa/b}$ denotes the distance from the source at b to the source at a, and $r_{ia/b}$ denotes the distance from the image source at b to the source at a. Substituting Eq. (14) into Eq. (6) gives

$$W = \mathbf{a}_{3\mathrm{D}}^{\mathrm{H}}\boldsymbol{q}\mathbf{H}^{\mathrm{T}}\mathbf{b}\mathbf{H}\boldsymbol{q}^{*}\mathbf{a}_{3\mathrm{D}} \tag{15}$$

The term $\mathbf{a}_{3\mathrm{D}}$ in this case is the 3D multipole amplitudes. To enable acoustic measurement of the 3D multipole amplitudes, $\mathbf{a}_{3\mathrm{D}}$, we truncate Eq. (3) using n monopoles in a 3D array with m measurement points under consideration; the 3D multipole amplitudes can then be resolved using a matrix inversion or pseudo-inversion as follows:

$$\mathbf{a}_{3\mathrm{D}} = \boldsymbol{\Psi}_{3\mathrm{D}}^{-1}\mathbf{p} \tag{16}$$

The 3D modal filtering matrix, $\boldsymbol{\Psi}_{3\mathrm{D}}$, is defined by the matrix of transfer functions between the n multipoles and the m measurement points under consideration, and is given by

$$\boldsymbol{\Psi}_{3\mathrm{D}} = [\boldsymbol{\psi}_{13\mathrm{D}}\ \ \boldsymbol{\psi}_{23\mathrm{D}}\ \ \cdots\ \ \boldsymbol{\psi}_{n3\mathrm{D}}] = \begin{bmatrix} \psi_{13\mathrm{D}}(\mathbf{r}_1) & \psi_{23\mathrm{D}}(\mathbf{r}_1) & \cdots & \psi_{n3\mathrm{D}}(\mathbf{r}_1) \\ \psi_{13\mathrm{D}}(\mathbf{r}_2) & \psi_{23\mathrm{D}}(\mathbf{r}_2) & \cdots & \psi_{n3\mathrm{D}}(\mathbf{r}_2) \\ \cdots & \cdots & \cdots & \cdots \\ \psi_{13\mathrm{D}}(\mathbf{r}_m) & \psi_{23\mathrm{D}}(\mathbf{r}_m) & \cdots & \psi_{n3\mathrm{D}}(\mathbf{r}_m) \end{bmatrix} \tag{17}$$

To generate a given multipole pattern, the amplitude of the monopole sources are fixed to be equal. For example, considering eight monopole sources, and again consistently using the Hadamard matrix, the resulting eight 3D multipole radiation transfer functions are governed by the relationship,

$$\begin{aligned} &[\psi_{13\mathrm{D}}(\mathbf{r})\ \ \psi_{23\mathrm{D}}(\mathbf{r})\ \ \cdots\ \ \psi_{83\mathrm{D}}(\mathbf{r})]^{\mathrm{T}} \\ &= \begin{bmatrix} 1 & 1 & 1 & 1 & 1 & 1 & 1 & 1 \\ 1 & 1 & 1 & 1 & -1 & -1 & -1 & -1 \\ 1 & 1 & -1 & -1 & -1 & -1 & 1 & 1 \\ 1 & 1 & -1 & -1 & 1 & 1 & -1 & -1 \\ 1 & -1 & -1 & 1 & -1 & 1 & 1 & -1 \\ 1 & -1 & 1 & -1 & -1 & 1 & -1 & 1 \\ 1 & -1 & 1 & -1 & 1 & -1 & 1 & -1 \\ 1 & -1 & -1 & 1 & 1 & -1 & -1 & 1 \end{bmatrix} \begin{bmatrix} \dfrac{\mathrm{j}\omega\rho_0}{2\pi r_{s1}}\mathrm{e}^{-\mathrm{j}kr_{s1}} + \dfrac{\mathrm{j}\omega\rho_0}{2\pi r_{i1}}\mathrm{e}^{-\mathrm{j}kr_{i1}} \\ \dfrac{\mathrm{j}\omega\rho_0}{2\pi r_{s2}}\mathrm{e}^{-\mathrm{j}kr_{s2}} + \dfrac{\mathrm{j}\omega\rho_0}{2\pi r_{i2}}\mathrm{e}^{-\mathrm{j}kr_{i2}} \\ \vdots \\ \dfrac{\mathrm{j}\omega\rho_0}{2\pi r_{s8}}\mathrm{e}^{-\mathrm{j}kr_{s8}} + \dfrac{\mathrm{j}\omega\rho_0}{2\pi r_{i8}}\mathrm{e}^{-\mathrm{j}kr_{i8}} \end{bmatrix} \end{aligned} \tag{18}$$

It is straightforward to show that $\mathbf{A}_{a3\mathrm{D}}$ (in Eq. (13)) is not diagonal. Practically, this means that the 3D multipoles are not orthogonal contributors to the error criterion, and so a reduction in the amplitude of a given multipole will not necessarily produce a corresponding reduction in the error criterion (not dissimilar to radiation from structural modes [62–64]). The weighting matrix $\boldsymbol{A}_{a3\mathrm{D}}$ will, however, be symmetric, and so can be diagonalised using an orthonormal transformation:

$$\boldsymbol{A}_{a3\mathrm{D}} = \boldsymbol{Q}\boldsymbol{\Lambda}\boldsymbol{Q}^{-1} \tag{19}$$

where the columns of $\boldsymbol{Q}$ are the eigenvectors of $\boldsymbol{A}_{a3D}$ and $\boldsymbol{\Lambda}$ is a diagonal matrix of the associated eigenvalues. It is then transformed/diagonalised quantities that are used in the sensing system design.

Combining all of this into the same form as Eq. (1), the radiated power can be written as

$$W \approx \boldsymbol{p}^{H}\left\{\boldsymbol{\Psi}_{3D}^{-1}\right\}^{H}\boldsymbol{Q}\boldsymbol{\Lambda}\boldsymbol{Q}^{-1}\boldsymbol{\Psi}_{3D}^{-1}\boldsymbol{p} \tag{20}$$

With this decoupling the modal filtering weights are now defined by $\boldsymbol{Q}^{-1}\boldsymbol{\Psi}_{3D}^{-1}$, the resolved signals (measured quantities/error signals) are then written as

$$\boldsymbol{a}_{3D} = \boldsymbol{Q}^{-1}\boldsymbol{\Psi}_{3D}^{-1}\boldsymbol{p} \tag{21}$$

The modal filter weights $\boldsymbol{Q}^{-1}\boldsymbol{\Psi}_{3D}^{-1}$ can be re-expressed as $\boldsymbol{Q}^{-1}\boldsymbol{\Psi}_{3D}^{-1} = \boldsymbol{N}\boldsymbol{\Psi}_{n3D}^{-1}$, where $\boldsymbol{N}$ is a diagonal matrix of frequency-dependent terms, and $\boldsymbol{\Psi}_{n3D}^{-1}$ is a normalised version of $\boldsymbol{Q}^{-1}\boldsymbol{\Psi}_{3D}^{-1}$ with the maximum coefficient amplitude equal to 1. The modal filter weights are defined by $\boldsymbol{\Psi}_{n3D}^{-1}$ and the measured quantities (error signals) become

$$\boldsymbol{a}_{3D} = \boldsymbol{\Psi}_{n3D}^{-1}\boldsymbol{p} \tag{22}$$

Eq. (22) gives precisely what was sought after, as proposed in Eq. (1). The weighting term, $\boldsymbol{\Lambda}$, is diagonal, meaning that the states defined by $\boldsymbol{\Psi}_{n3D}^{-1}\boldsymbol{p}$ are independent contributors to radiated power.

2.2. The 2D decomposition approaches

In this section the 2D centric approaches to developing orthogonal radiation patterns are discussed. Though the target of this work is a 3D noise source we will compare approaches where the noise is modelled as a 2D one. Illustrated in Fig. 4 are three different approaches (power modes [36], radiation modes [37] and multipoles [25]) to developing orthogonal radiation patterns for 2D sources. For conciseness of the two structural approaches, where radiated power is decomposed based on structural modes [36] and structural elements [37], only the latter is considered here. A more expansive development and application to a 2D noise source with a 128 acoustic sensing array using both decompositions developments can be found in Refs. [48,49,73]. These articles also illustrate the many shared characteristics which the structural centric approaches have. The third, 2D approach, is also based on phased monopoles [25]. The technique is very similar to the development in the previous section, except the monopoles are arranged in a 2D array rather than a 3D array. Then the vector of radiation transfer functions is similar to Eq. (18), except the contribution from each of the image components of each monopole are dropped. The 2D development follows a similar procedure detailed in Eqs. (2)–(22), see Ref. [25] for more details.

In the decomposition of radiated power based upon a set of elemental radiators [37], the elemental radiators are approximated as elemental piston radiators, with each element having a radiation transfer

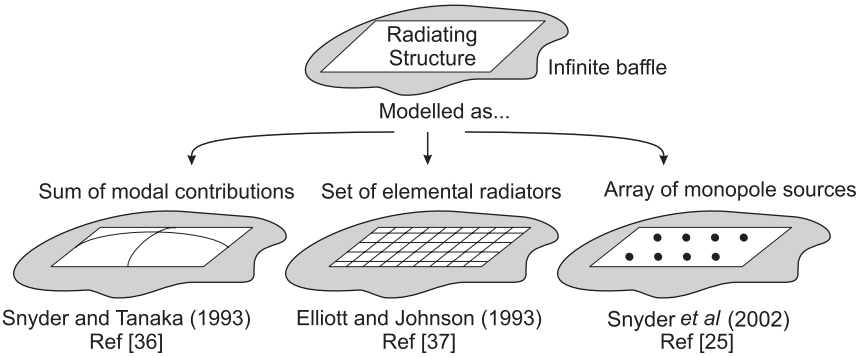

Fig. 4. Different modal filter approaches.

function defined as

$$\frac{\mathrm{j}\omega\rho_0 S}{2\pi r}\mathrm{e}^{-\mathrm{j}kr} \tag{23}$$

where S is the area of each elemental radiator, and r is the distance from the radiator to a position in the far field. The pressure immediately in front of each elemental source, $\mathbf{p}$, can be given by

$$\mathbf{p} = \mathbf{Z}\mathbf{v} \tag{24}$$

where $\mathbf{Z}$ is the matrix of acoustic impedances for the elemental radiators and $\mathbf{v}$ is the complex velocity of each elemental source. Thus radiated power can be rewritten in terms of elemental radiators, similar to Eq. (6) as,

$$W = \frac{S}{2}\mathrm{Re}[\mathbf{v}^{\mathrm{H}}\mathbf{p}] = \frac{S}{2}\mathrm{Re}[\mathbf{v}^{\mathrm{H}}\mathbf{Z}\mathbf{v}] = \mathbf{v}^{\mathrm{H}}\mathbf{R}\mathbf{v} \tag{25}$$

For a set of elemental radiators, the symmetric radiation resistance matrix is given by

$$\mathbf{R} = \frac{\omega^2\rho_0 S^2}{4\pi c_0}\begin{bmatrix} 1 & \frac{\sin kr_{1,2}}{r_{1,2}} & \cdots & \frac{\sin kr_{1,I}}{r_{1,I}} \\ \frac{\sin kr_{2,1}}{r_{2,1}} & 1 & & \vdots \\ \vdots & & \ddots & \\ \frac{\sin kr_{I,1}}{r_{I,1}} & \cdots & & 1 \end{bmatrix} \tag{26}$$

where $r_{i,j}$ is the distance from element i to j and the total number of element radiators considered is I. The radiation mode shapes are then simply the eigenvectors of Eq. (26). The equation for radiated power can then be written as

$$W = \mathbf{v}_R^{\mathrm{H}}\mathbf{R}\mathbf{v}_R = \mathbf{v}_R^{\mathrm{H}}\mathbf{Q}_R\mathbf{\Lambda}_R\mathbf{Q}_R^{\mathrm{T}}\mathbf{v}_R \tag{27}$$

where $\mathbf{Q}_R$ are the eigenvectors and $\mathbf{\Lambda}_R$ the eigenvalues the $\mathbf{R}$ matrix, and $\mathbf{v}_R$ is the vector of elemental velocities. This development of radiated power takes on the same form as Eq. (1). The measured states $\mathbf{a}_R$, which are solely vibration based, for this formulation are then

$$\mathbf{a}_R = \mathbf{v}_R^{\mathrm{H}}\mathbf{Q}_R \tag{28}$$

From the proceeding equations, one can observe that the structural centric approach is restricted to vibration measurement and requires modification for measurement in the acoustic domain. Modification can be achieved by relating pressure measurements (using an acoustic sensing system) back to the velocity states of a vibrating source which inherently these methods were designed to measure. The radiated pressure from a vibrating source can be written as

$$p(\mathbf{r}) = \mathbf{Z}\mathbf{v}_R \tag{29}$$

where $\mathbf{Z}$ is the vector of radiation transfer functions and $\mathbf{v}_R$ is the corresponding vector of vibration states. The radiation transfer function between radiated pressure and elemental velocity takes on a matrix form and can be written as

$$\mathbf{Z}_R = \begin{bmatrix} \frac{\mathrm{j}\omega\rho_0 S}{2\pi r_{1-1}}\mathrm{e}^{-\mathrm{j}kr_{1-1}} & \frac{\mathrm{j}\omega\rho_0 S}{2\pi r_{1-2}}\mathrm{e}^{-\mathrm{j}kr_{1-2}} & \cdots & \frac{\mathrm{j}\omega\rho_0 S}{2\pi r_{1-M}}\mathrm{e}^{-\mathrm{j}kr_{1-M}} \\ \frac{\mathrm{j}\omega\rho_0 S}{2\pi r_{2-1}}\mathrm{e}^{-\mathrm{j}kr_{2-1}} & \frac{\mathrm{j}\omega\rho_0 S}{2\pi r_{2-2}}\mathrm{e}^{-\mathrm{j}kr_{2-2}} & & \vdots \\ \vdots & & \ddots & \vdots \\ \frac{\mathrm{j}\omega\rho_0 S}{2\pi r_{N-1}}\mathrm{e}^{-\mathrm{j}kr_{N-1}} & \cdots & \cdots & \frac{\mathrm{j}\omega\rho_0 S}{2\pi r_{N-M}}\mathrm{e}^{-\mathrm{j}kr_{N-M}} \end{bmatrix} \tag{30}$$

where N is the number of elemental radiators and M is the number of acoustic measurement locations. The distance r_{i-j} in this expression is the distance from the ith elemental to the jth microphone location. The velocity states of the panel can then be rewritten in terms of pressure:

$$\mathbf{v}_R = \mathbf{p}\mathbf{Z}_R^{-1} \tag{31}$$

Thus Eq. (27) can be written in terms of pressure rather than velocity:

$$W = \mathbf{p}^{\mathrm{H}}(\mathbf{Z}_R^{-1})^{\mathrm{H}}\mathbf{Q}_R\mathbf{\Lambda}_R\mathbf{Q}_R^{\mathrm{T}}\mathbf{Z}_R^{-1}\mathbf{p} \tag{32}$$

2.3. State contribution to radiated power

By selecting only a handful of important states to control, a reduction in the accuracy of the error may result; however, truncating the number of signals to be controlled leads to a faster convergence and more robust control system. The question then becomes: how many signals are required to achieve the maximum amount of attenuation, over a prescribed frequency range, for a given control setup? To examine this question, recall that the importance of each state, a resolved signal (decomposed mode), is described by its eigenvalue (of the global performance matrix $\mathbf{A}_{a3\mathrm{D}}$, and $\mathbf{R}$) as this value is proportional to each states radiation efficiency. By then looking at the relative eigenvalues the designer can gain insight to the required number of states for a given frequency range.

To compare eigenvalues of each of the decomposition developments in Section 2, of this article, consider a noise source with dimensions 0.35 m × 0.85 m × 0.6 m (x, y, z). These dimensions are identical to those of the noise source which is the subject of the experimental investigation later in this article.

For the considered noise source, ''virtual'' monopoles are evenly distributed over the source in a 3D array (as illustrated in Fig. 5), and a 2D array as (illustrated in Fig. 6). In the radiation mode development the panel is divided up with 20 elements along the x-dimension and 40 elements along the y-dimension.

The eigenvalues of the square weighting matrix for each of the three different approaches (3D and 2D multipoles, and radiation modes) are plotted in Figs. 7–9. Observe that the relative values of the eigenvalues, at low frequencies, suggest that only 1–3 signals need to be considered to obtain an accurate estimate of power,

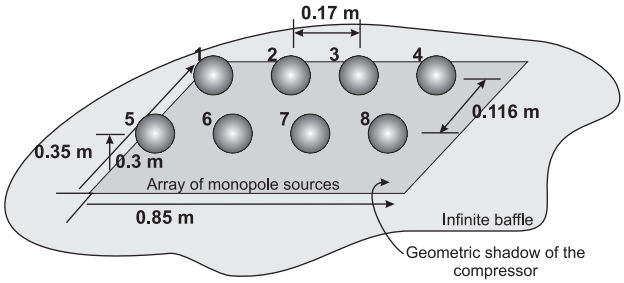

Fig. 5. Arrangement for the 3D array of monopole sources.

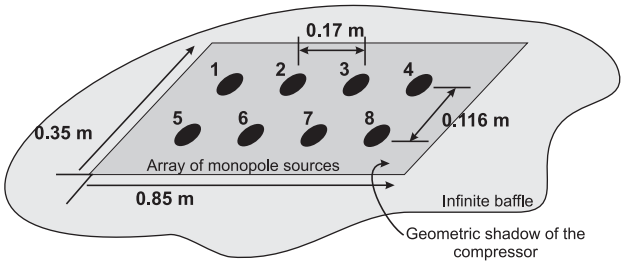

Fig. 6. Arrangement for the 2D array of monopole sources.

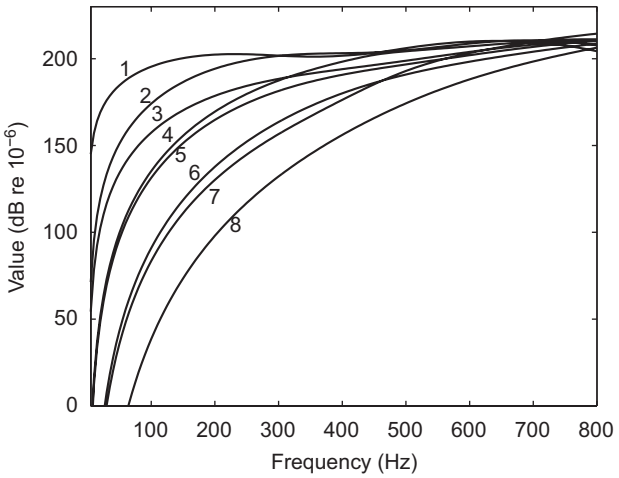

Fig. 7. Eigenvalues of the weighting matrix $\mathbf{A}_{a3D}$ for the 3D multipole formulation, plotted as a function of frequency.

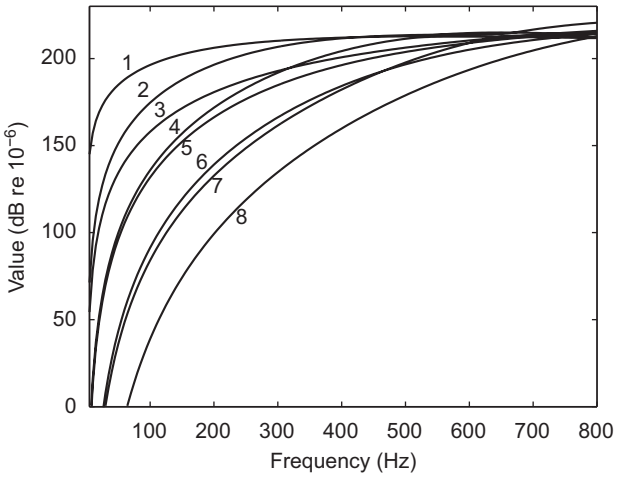

Fig. 8. Eigenvalues of the weighting matrix $\mathbf{A}_{a2D}$, for the 2D multipole formulation, plotted as a function of frequency.

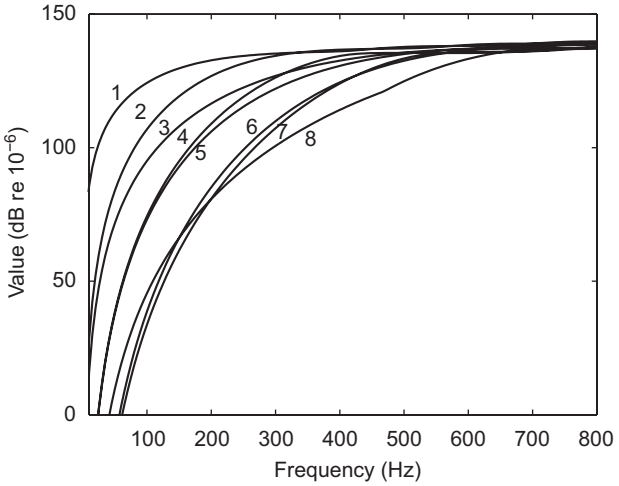

Fig. 9. Eigenvalues of the weighting matrix $\mathbf{R}$, for the radiation mode formulation, plotted as a function of frequency.

as the residual eigenvalues (following truncation) are small in comparison. Another interesting observation is that the speed of eigenvalue convergence is slower for the multipole development.

2.4. Inverse considerations

In all of the above decomposition developments, an inverse operation is necessary to find the modal filtering weights facilitating evaluation of the different orthogonal constituents. Wherever an inverse is used, the accuracy of the reconstruction is often determined by the conditioning of the matrix to be inverted in the estimation process.

The important matrices in terms of practical measurement of orthogonal contributors for each decomposition in this work are: $\mathbf{\Psi}_{n3\mathrm{D}}$ and $\mathbf{Z}_R$. It is straightforward to show that when a large sensing array, of the form illustrated in Fig. 1, is placed at distances greater than a few metres from a noise source of a similar size to the one considered in the following section, the condition number for full matrices, $\mathbf{\Psi}_{n3\mathrm{D}}$ and $\mathbf{Z}_R$ is poor. This is due to the decay in the exponential radiation transfer function ($\mathrm{e}^{-\mathrm{j}kr}$) and the small variation in the distance from the elemental radiators to each of the sensors.

There is a large amount of literature on methods to overcome ill-conditioned matrices in acoustics [65–69]. However, the columns of the final matrices to be inverted ($\mathbf{\Psi}_{n3\mathrm{D}}$ and $\mathbf{Z}_R$) contain columns of constituents, which are independent contributors to the total acoustic power. Total power can be written in terms of the individual *independent* constituent (3D multipole, 2D multipole or radiation mode),

$$W_{\text{total}} = \sum_{i=1}^{L} W_{i\text{th constituent}} \tag{33}$$

Taking the 3D multipole case as an example, the power in each multipole can then be written as

$$W_{i\text{th multipole}} = \mathbf{\Lambda}(i,i)[\mathbf{\Psi}_{n3\mathrm{D}}^{-1}(:,i)\mathbf{p}]^2 \tag{34}$$

where $\mathbf{\Lambda}(i,i)$ is the ith multipole radiation efficiency, $(:,i)$ represents all rows of the ith column and $\mathbf{p}$ is the vector of measured pressure amplitudes. Since each constituent is independent, this enables the use of a pseudo-inverse on each column of the modal filter matrix, $\mathbf{\Psi}_{n3\mathrm{D}}^{-1}$ and $\mathbf{Z}_R^{-1}$, bypassing any inverse problems (as a single columned matrix cannot be ill-conditioned). This manipulation will be used in the following experimental investigation.

3. Experimental implementation

The noise source used in the experimental investigation in this work is a 1.8 kW air compressor. Such a source represents significant challenges to typical state of the art global sensing strategies which are formulated in the structural domain and typically 2D. The compressor is placed in an anechoic chamber on a hard surface. Referring to Fig. 10, the compressor has a width of 0.35 m, length of 0.85 m and a height of 0.6 m. The aim of the experiments is simply to measure radiated power using the modal filtering technique and compare the estimates to the actual radiated power. As described previously, if radiated power can be accurately observed using a limited set of inputs, then a range of control techniques may be applied to provide disturbance attenuation. It is worth noting that in a practical active noise control system, the actual level of global attenuation which is achievable depends on a range of factors, most importantly being the number, type and location of the secondary sources [47,48,70–72]. Therefore it is not crucial if a sensing system provides a signal with an error (compared to the true cost function being minimised) of a few dB at a spectral peak, as long as (at a very minimum) the spectral peak is clearly visible above the noise floor. The goal then for a practical sensing system is to pick up as many peaks, as close as possible to the real (global) error. When discussing the experimental results these practical points are kept in mind, resulting in some data spoken of more positively than it may appear from a mathematical view of the raw numbers.

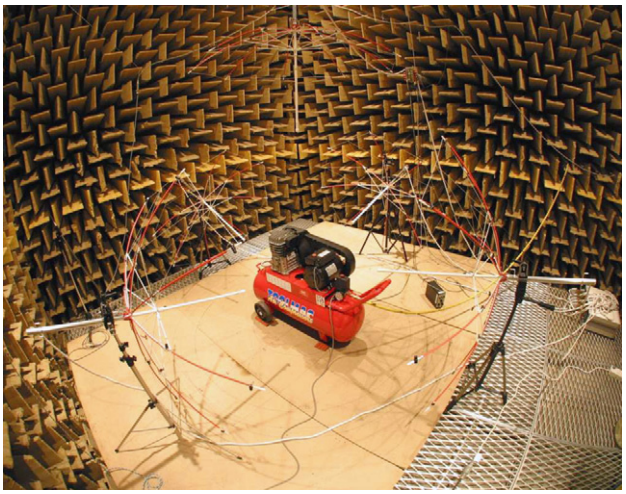

Fig. 10. The air compressor and five microphone arrays in the anechoic chamber.

To determine the *actual* radiated power of the compressor, pressure over the frequency range 5–800 Hz was measured at 0.25 Hz increments at 45 locations over a hemisphere with radius of 1.2 m from the compressor. From these pressure measurements sound power was determined [8]. The aim of the experiments is to assess the usefulness of the new strategy for sensing the global error for 3D sources based on 3D orthogonal multipoles. Also examined is the use of 2D sensing strategies for the 3D source. The experiments examining these points take the following sequence:

1. Decomposition of the radiated sound field into radiation patterns based on a 3D array of monopoles. The summed result is compared to the actual level of radiated power.
2. Decomposition of the radiated sound field into radiation patterns based on a 2D array of monopoles. The summed result is compared to the actual level of radiated power.
3. Decomposition of the radiated sound field into radiation patterns based on radiation modes. The summed result is compared to the actual level of radiated power.

To decompose the radiated sound field from the compressor into radiation modes, it has been assumed that the compressor radiates noise like a rectangular panel, the size of which was based on the geometric shadow (length multiplied by the width) of the compressor.

Since the noise source being studied here is 3D, multiple microphone arrays are required for the experiment so that radiated noise can be measured in several directions. Five arrays each consisting of 16 microphones were constructed. The 80 microphone signals interfaced to a custom built I/O modal filtering system. The modal filtering system was built using (low-cost) Analog Devices AD1845JST 16 bit stereo codecs, interfacing to an Analog Devices ADSP21062 EZKIT. Once designed, the component cost of constructing the modal filtering system is a few thousand dollars, a price tag that can be justified for large active noise control problems (e.g. a substation transformer). Using codecs, the system is also capable of 128 outputs. With the modal filtering weights being fixed values, as described in the previous section, the single low-cost DSP can perform the required calculations at a sample rate of 5.5 kHz.

Referring again to Fig. 10, the five 16 element microphone arrays were placed at a distance of 1.2 m from all four sides and above the compressor. This was the maximum possible distance from the compressor due to the size of the wooden boards and the dimensions of the anechoic chamber. The anechoic chamber used for the experiments has dimensions 4.75 m × 3.9 m × 3.94 m. A sketch of the experimental setup and the procedure to calculate the constituents of each decomposition approach is illustrated in Fig. 11.

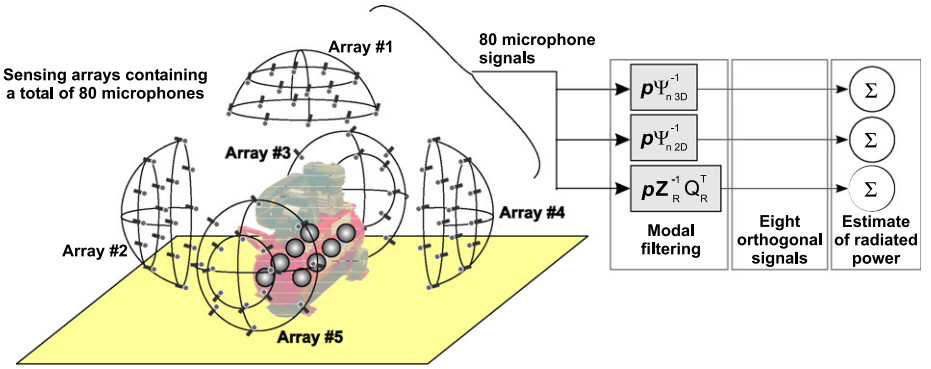

Fig. 11. Sensing experiment overview.

4. Sensing radiated power from an air compressor

4.1. The 3D multipole decomposition

In the 3D decomposition used in this section, the air compressor has been modelled as a 3D array containing eight "virtual" monopoles. The monopoles are evenly spaced over the geometric shadow of the compressor, at a height of 0.3 m above the hard surface, which the compressor is sitting on. The monopole arrangement is illustrated in Fig. 5. Transfer functions between the microphones and "virtual" monopoles (required for the modal filtering weights, see Eqs. (18)–(22)) are simply calculated based on distances, as illustrated in Fig. 3, however it is worth reiterating that the outcome of the modal filtering exercise is the amplitude of the orthogonal multipole radiation patterns.

To examine this decomposition method and its implementation the following factors have been varied:

- the discrete frequency at which the multipole modal filtering weights are calculated; and
- the number of resolved signals (3D multipoles) used to examine sound power (the global error criterion).

The number of "virtual" monopoles used to generate the multipole radiation patterns has been kept constant at eight in this section.

Illustrated in Fig. 12 is the estimation of radiated power from the first, first three and all eight multipole(s) based on modal filtering weights calculated at 50 Hz (Fig. 12(a)) and 200 Hz (Fig. 12(b)). For comparison the actual radiated power, as calculated from 45 pressure measurements is also plotted. This signal appears in all of the following figures containing experimental data. In the experimental data figures in this section, and throughout the paper, peaks in the actual sound power spectrum are marked with stars (only peaks above 55 dB); the corresponding peak in the estimates of radiated power are also marked. For clear comparison the values of the peaks are recorded within tables. The peaks in the radiation spectrum correspond to the rotational speed of the air compressors motor and the corresponding harmonics.

Observe in Fig. 12(a) and (b) that even with just one multipole signal the estimate of radiated sound power would be useful over lower frequencies (particularly at spectral peaks) for a practical active noise control implementation. At higher frequencies the estimate contains the spectral peaks but exhibits some error in amplitude. These conclusions are supported by Table 1, which contains the values of the spectral peaks for the actual sound radiation and the different estimates from the modal filtering process. The experimental data in Fig. 12 and Table 1 show an increase in accuracy of the sound power estimate at the peeks as the number of multipoles increases. The improvement in the estimate of sound power between one and three multipoles is much more significant than the change from three to eight multipoles in the majority of peaks.

It is important to note that should the decomposed quantities be used as error signals in an active noise control system, errors away from the spectral peaks would carry less weight as little energy is contained here; and it will be the number of actuators and their location which will have greater influence on the achieved

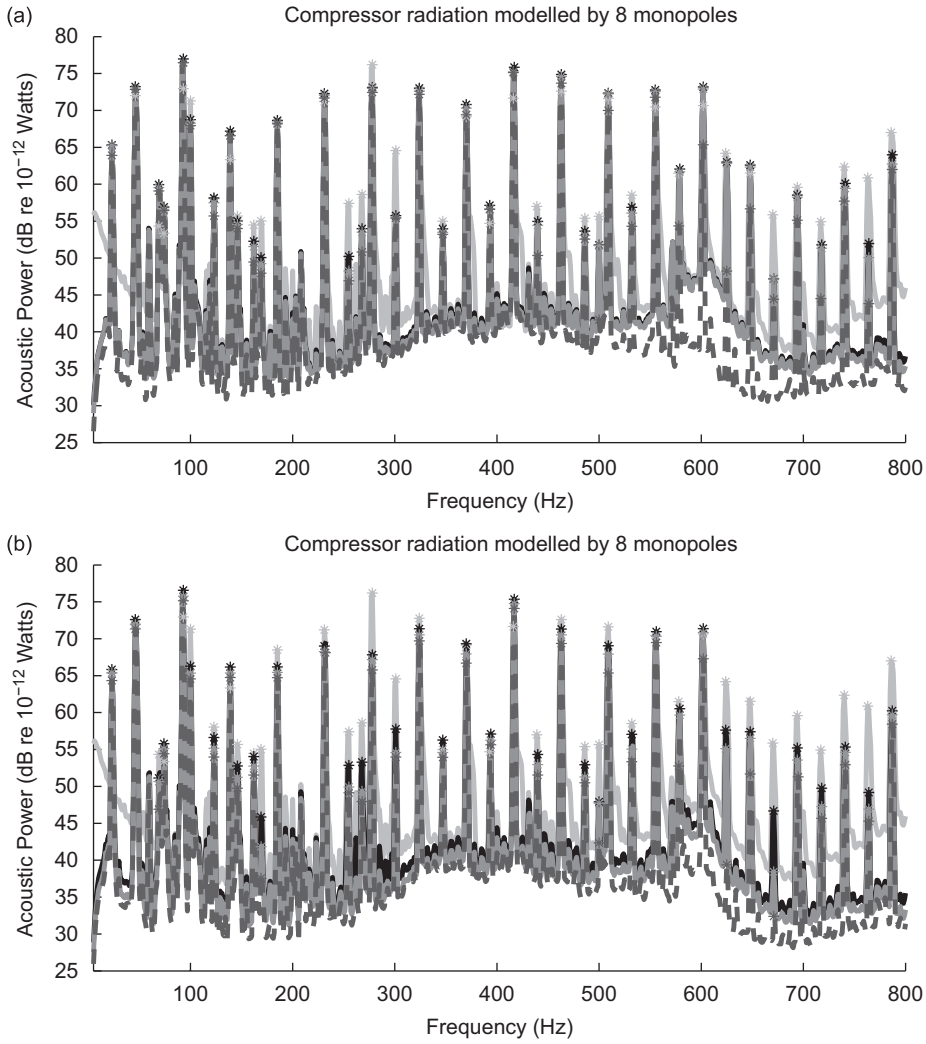

Fig. 12. Estimate of radiated power based on a 3D multipole decomposition: (a) weights calculated at 50 Hz, (b) weights calculated at 200 Hz. ---- One "3d" multipole, ——— three "3d" multipoles, ——— eight "3d" multipoles, ——— actual power.

attenuation (absolute amount and the frequency range) than the error signal of the quality shown in Fig. 12(a) and (b). Observe in Fig. 12 and Table 1 that there is very little difference between the three multipole and eight multipole estimates of radiated power, especially for the estimates using modal filtering weights evaluated at 50 Hz. The results suggest that just three signals would be required to give an estimate of radiated power over the frequency range 5–800 Hz suitable for an attempt at active noise control.

4.2. The 2D multipole decomposition

Illustrated in Fig. 13 is the conceptual arrangement of the monopoles used in the decomposition process studied in this section. For the decomposition of radiated power here we model the air compressor based on a 2D array of eight "virtual" monopoles. The "virtual" monopoles are evenly distributed over the geometric shadow of the compressor (placed on the hard floor), as illustrated in Fig. 6.

In the investigation of this decomposition method, only the number of resolved signals (2D multipoles) used to estimate sound power (the global error criterion) has been varied. The number of monopoles used to generate the multipole radiation patterns remains constant at eight in this section.

Table 1
Sound power at peak frequencies plotted in Section 4 (peaks above 55 dB in the actual spectrum)

Peak freq. (Hz)	Actual power	Decomposition technique											
		3D multipoles (Section 4.1)						2D multipoles (Section 4.1)			Radiation modes (Section 4.3)		
		50 Hz weights			200 Hz weights			50 Hz weights			50 Hz weights		
		1 multi	3 multi	8 multi	1 multi	3 multi	8 multi	1 multi	3 multi	8 multi	1 modes	3 modes	8 modes
23	65.33	63.90	65.22	65.30	64.33	65.40	65.84	58.76	60.72	63.22	65.06	66.54	67.62
46	72.01	72.85	72.86	73.23	71.33	71.93	72.61	61.54	68.33	70.47	63.59	64.72	65.88
69	54.33	59.08	59.56	59.95	46.89	50.65	51.12	51.85	58.41	61.11	61.79	63.02	64.19
74	53.37	56.44	56.60	56.90	54.42	55.11	55.79	53.84	57.81	60.04	56.93	57.47	58.24
93	72.95	76.46	76.48	76.97	75.15	75.77	76.57	67.14	74.23	76.70	73.87	74.44	75.12
100	71.30	67.94	68.28	68.74	64.56	65.34	66.29	63.57	68.12	71.90	69.17	69.78	70.43
123	58.03	55.70	57.48	58.14	53.99	55.16	56.62	45.10	54.18	57.97	47.62	48.93	49.82
139	63.34	66.57	66.59	67.19	64.75	65.36	66.16	42.73	60.75	64.41	61.16	62.69	63.63
146	55.68	54.00	54.54	55.03	49.74	51.24	52.77	51.52	54.24	57.57	51.13	52.25	53.07
162	54.46	49.46	51.56	52.28	51.53	52.75	54.04	49.36	51.76	56.56	44.33	46.27	47.10
169	55.02	47.94	49.24	50.06	37.55	41.84	45.85	46.00	55.03	57.16	53.04	53.39	53.98
185	68.48	68.19	68.27	68.64	64.73	65.45	66.18	65.09	67.22	69.07	63.44	64.01	65.32
231	71.21	71.67	72.05	72.28	68.12	68.25	69.01	67.95	70.09	72.32	69.76	70.31	71.04
255	57.41	46.93	48.24	50.23	49.14	49.91	52.84	60.66	60.68	60.69	47.49	48.99	50.32
268	58.60	50.81	53.49	53.98	47.94	49.34	53.28	59.31	59.91	60.85	47.64	48.83	50.26
278	76.19	72.44	73.00	73.11	65.78	67.16	67.83	77.09	77.82	78.69	72.71	73.59	74.74
301	64.56	55.41	55.45	55.74	53.97	54.59	57.76	62.82	63.31	63.73	54.02	55.88	57.61
324	72.77	72.18	72.59	73.01	69.70	70.54	71.35	64.80	67.81	70.61	65.84	65.98	66.22
347	54.97	53.21	53.48	53.95	53.93	54.59	56.26	52.60	54.24	55.36	49.55	49.82	50.62
370	69.14	69.40	70.31	70.80	66.69	67.94	69.33	58.22	68.28	73.52	64.52	66.14	66.91
393	54.68	56.58	56.67	57.14	55.64	56.26	57.09	40.54	52.00	55.34	52.81	53.96	54.95
416	71.66	75.12	75.24	75.85	74.11	74.75	75.36	67.47	73.47	75.91	70.43	71.64	73.12
439	56.99	50.34	54.44	54.96	51.54	52.96	54.32	50.87	53.98	58.41	46.44	47.05	48.15
463	72.61	73.70	74.60	74.86	69.36	70.52	71.31	70.92	73.13	75.95	70.48	70.90	71.24
486	55.39	52.56	53.07	53.64	50.50	51.26	52.92	43.72	45.90	54.02	45.57	47.97	48.53
500	55.66	41.63	51.68	51.76	42.34	47.72	47.91	45.53	51.19	61.15	49.03	49.22	50.19
509	71.62	70.00	72.24	72.35	65.37	67.93	69.06	69.82	71.12	74.64	68.19	68.68	69.75
532	58.51	54.31	56.08	56.86	53.33	55.04	57.06	48.21	49.70	54.32	45.73	46.80	47.76
555	70.48	71.78	72.54	72.76	69.48	70.33	70.96	60.75	65.54	72.38	66.52	66.60	68.37
578	61.48	54.34	61.70	62.05	52.77	59.66	60.52	54.67	55.55	65.91	48.09	48.45	49.37
602	70.66	65.35	72.92	73.19	67.30	70.85	71.37	67.09	68.52	74.69	55.20	56.18	57.41
624	64.19	48.23	62.82	63.01	39.37	54.87	57.62	56.50	57.41	66.29	59.10	59.13	60.18
648	61.53	56.66	62.33	62.60	51.68	56.50	57.41	53.80	55.57	63.45	52.42	52.92	54.26
670	55.87	44.41	47.17	47.19	32.40	38.42	46.67	48.13	50.26	52.66	45.98	48.25	49.86
694	59.57	55.13	58.24	58.54	51.28	53.56	55.21	52.65	53.21	59.33	45.05	45.13	46.62
717	54.93	44.49	51.33	51.79	45.68	47.27	49.76	41.70	48.09	56.01	37.05	37.64	39.18
740	62.35	57.71	59.44	60.12	52.93	54.61	55.33	58.05	58.10	61.12	48.01	49.37	49.84
763	60.86	43.82	50.05	51.97	45.27	46.93	49.17	51.17	55.57	60.36	42.53	42.93	46.78
786	67.00	62.01	62.73	63.98	58.42	59.71	60.24	56.35	62.89	66.65	56.38	57.25	58.77

Peak data are in dB re 10^{-12} W.

Illustrated in Fig. 14 is the estimation of radiated power from the first, first three and all eight multipole(s), using modal filtering weights calculated at 50 Hz. The peak values marked by stars are shown in Table 1. Observe that these estimates of the global error (sound power) would provide useful error signals (more so at lower frequencies) for a practical active noise control implementation. At higher frequencies the estimate contains the spectral peaks yet with some error in amplitude. While the decomposition of the sound field is based on a 2D approximation of the sound source, the resulting multipole signal would again provide a useful

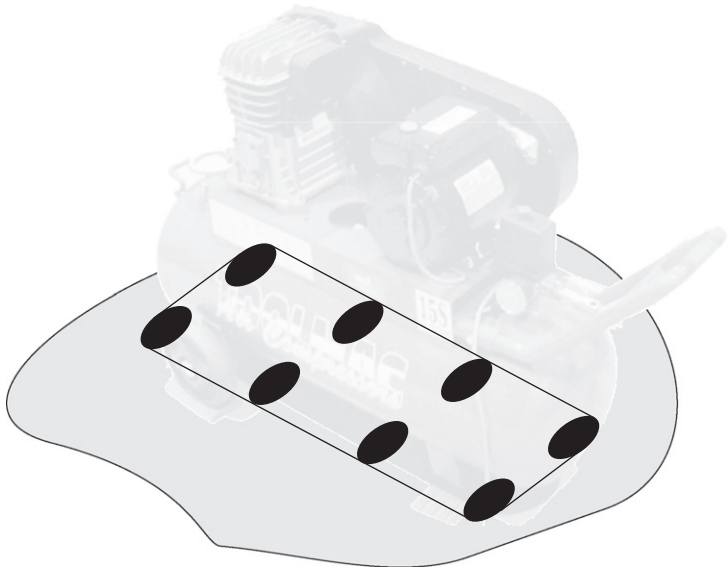

Fig. 13. Compressor modelled as a 2D array of monopole sources (sources situated on the hard surface beneath the compressor).

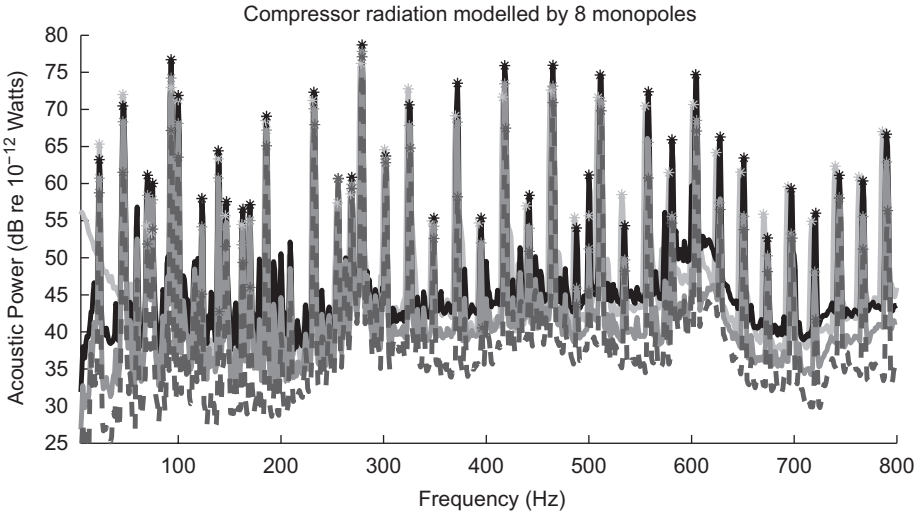

Fig. 14. Estimate of radiated power based on a 2D multipole decomposition. ---- One "2d" multipole, ——— three "2d" multipoles, ——— eight "2d" multipoles, ——— actual power.

error for an active noise control system as the measure contains the majority of the spectral peaks and the level of attenuation achieved would be predominately influenced by the type, number and location of secondary sources. When considering three (2D) multipoles using modal filtering weights calculated at 50 Hz, observe the improvement over just considering one multipole in the estimate of radiated power at higher frequencies. Visual inspection of the broadband results suggests that just three signals are required to give a fairly practical estimate of radiated power over the frequency range 5–800 Hz.

In comparison to the decomposition of radiated power based upon a 3D array of monopoles, presented in the previous section, the estimates of radiated power in this section appear rather similar. The similarity shows that a 2D array of monopoles is capable in some form of decomposing a sound field of the 3D source under

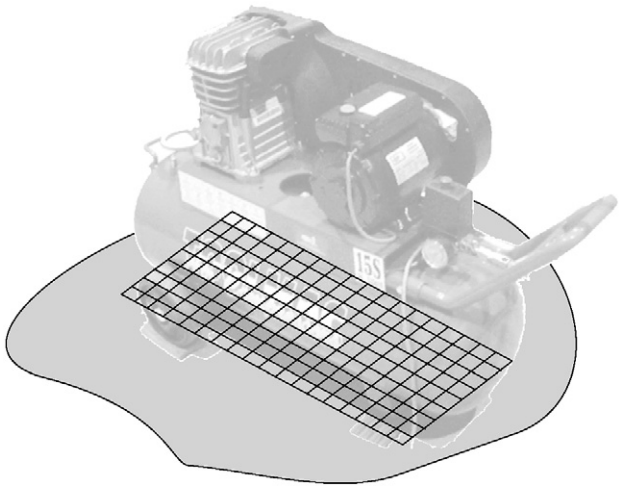

Fig. 15. Compressor modelled as an array of elemental radiators (placed on the hard surface beneath the compressor).

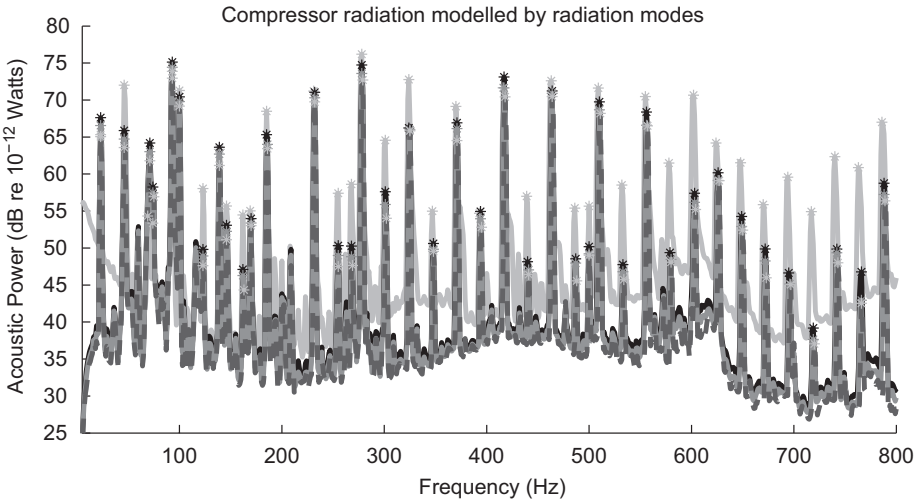

Fig. 16. Estimate of radiated power based on a radiation mode decomposition. - - - - One radiation mode, ——— three radiation modes, ——— eight radiation modes, ——— actual power.

investigation. It also illustrates there are some similarities between the 2D and 3D multipole decomposition methods.

4.3. Radiation mode decomposition

In this section, acoustic radiation of the air compressor is modelled as a rectangular panel, which was divided up into elemental radiators, conceptually shown in Fig. 15. The size of the panel is based on the length and width of the compressor (its geometric shadow). Structurally the link between a rectangular panel and an air compressor is weak. However, the purpose of these experiments is to test if a 2D radiation mode decomposition of radiated power can be used to obtain a useful estimate of a global error for a 3D, non-structural noise source. To calculate the filtering weights to resolve the radiation modes, the *conceptual* panel is divided densely up into 800 elements.

In the investigation of this decomposition method only the number of resolved signals (radiation modes) used to estimate sound power (the global error criterion) has been varied.

The maximum number of radiation modes was restricted to eight so that the number of resolved signals would be the same as in the previous two sections which dealt with the 3D and 2D multipole decomposition. Illustrated in Fig. 16 is the estimation of power from only the first radiation mode based on modal filtering weights calculated at 50 Hz. The values at the spectral peaks are contained in Table 1. Observe that the radiation mode decomposition gives a practical estimate of sound power up to approximately 550 Hz, as the majority of the peaks up to this frequency have been captured. Above 550 Hz most spectral peaks are visible; however, they contain higher levels of errors.

Considering all eight radiation modes, the accuracy of the decomposition is noticeably less in comparison to the other two decomposition methods when also considering eight resolved, especially at high frequencies. Observe that there is only a slight improvement over the spectrum when all eight modes are considered. This result suggests that more than eight radiation modes are likely to be required to give an accurate estimate of radiated power over the frequency range 5–800 Hz.

4.4. Discussion of results

The aim of the experiments was to assess the usefulness of the new strategy for sensing the global error for 3D sources based on 3D orthogonal multipoles. The results in Section 4.1 clearly showed that the sensing strategy was capable of producing a practical estimate of the global error.

The decomposition of the 3D noise source using 2D approaches also yielded estimates of the radiated power which would be useful in a practical active noise control implementation. This result was achieved despite the oversimplification of the source—a point equally applicable to both 2D strategies. Experimental results showed that when considering the first constituent (orthogonal signal), of the two, 2D strategies the radiation mode technique returned a more accurate estimate at the lower frequency peaks. At higher frequencies, this result was reversed. The poorer performance at higher frequencies is likely due to the radiation mode technique requiring more orthogonal constituents at higher frequencies to account for all for the radiated power as shown in Ref. [48]. However, caution should be taken when suggesting one technique is fundamentally better than another, as any difference in achieved attenuation in a practical implementation may be negligible [49].

One result in common with all the radiated power decompositions is that the accuracy of the estimate is not greatly improved by increasing the number of resolved constituents from three to eight. Where there was a large change at spectral peaks of radiated power (from three to eight constituents), in most cases the estimate was still relatively far from the actual sound power to begin with.

It is also worthwhile mentioning the sources of errors within the experimental work. These sources will inherently influence the results; however, every attempt was made to minimise their effect.

In some of figures a very small shift in frequency of the peak (at higher frequencies only) can be noticed. This is likely due to the effect of temperature increases within the anechoic chamber on both the microphones and the compressor itself as the room heats up after constant running.

Guidelines for tests in anechoic chambers are suggested in Ref. [8]. The distances from the microphones to the source and the walls are important factors. In our experiments the location of the microphones were limited by the size of the floor hard surface as mentioned earlier. Other sources of errors in the experiments relating to the equipment include phase and amplitude mismatch of the 80 microphones. The sensing strategy assumes ideal error sensors; however, each of the 80 microphones has a different dynamic response. The microphones were calibrated at 200 Hz, as at the beginning this frequency was thought to be approximately in the middle of the frequency range where the modal filtering strategy would be effective. Analysis showed that over the frequency range 20–400 Hz the average variation in sound pressure amplitude for the 80 microphones was close to 1 dB (re 20 μPa) with a maximum variation of 3 dB. Phase variations between the sensors also exist, which is not ideal for the real-time sensing procedure used. However, analysis indicated that over the frequency range 20–400 Hz the average variation in phase for the 80 microphones was close to 2°.

Another possible source of errors in the experiment is due to the physical arrangement, specifically the spatial inhomogeneity of the error sensors over the source. While a large number of microphones are used and placed in five different planes, the coverage of the noise source with the microphones is still non-uniform.

As more microphones are used the errors associated coverage are minimised; in these experiments a very large number of microphones (80) are used.

The experiments also contain errors related to the mismatch between assumed geometry and actual geometry of the sound source. There is little doubt that this is present in someway in the experiments as the entire air compressor is considered as the source; however, it could be just the motor (for example) which is the dominant source of the noise, meaning the cylinder containing the compressed air, and other parts are less important. Perhaps a greater density of monopoles could be placed in regions which are more responsible for radiated noise. It is expected that as the number of monopoles used in the decomposition process increases the effect of this error is minimised—this is partly the purpose of the investigation in the next section. The precise characteristics of the source were not investigated. This is exactly the point of the generalised approach—to treat all sources in the same way and sense the global error in a generalised fashion, removing costly and difficult analysis which may or may not be conclusive. The result is a significant simplification of sensing methodologies for the sensing of a global error, sound power. The sensing strategy makes the assumption that radiation from all sources can be written as the sum of orthogonal multipole radiation amplitudes. It is this assumption that has been checked experimentally in this work: the results indicate that in terms of practical active noise control implementation a very useful estimate of radiated power based on just a few orthogonal signals over a broad frequency range is available, a conclusion which holds in practice even with the uncertainty from the errors mentioned and discussed in this section.

5. Using additional monopoles in the decomposition

In the previous section, decomposition of the radiated acoustic field based on both 3D and 2D monopole arrays was shown to produce a practical set of error signals that could be used in an active control implementation. In this section, further aspects of the multiple decomposition are examined experimentally. Firstly, more monopoles, spread over the air compressor, are used in the decomposition process. Secondly, the effect of different spatial arrangements using a large number of monopoles used in the decomposition process is examined.

The radiated field of the air compressor in this section is decomposed into multipoles based on different arrangements of 16 monopoles, an increase over the previous section. Illustrated in Fig. 17 are the three, 3D monopole arrangements to be used in the decomposition process. Of interest here is the effect of the monopole arrangement within the array on the accuracy of the estimate of radiated power.

The previous sections showed that eight resolved signals can provide a useful estimate of radiated power. Consequently, and also to allow for comparison to results in earlier sections, the maximum number of multipoles (resolved orthogonal constituents) considered in the decompositions is eight.

Plotted in Fig. 18(a)–(c) is the estimate of sound power considering the first and all eight multipole(s) based on the three, 3D monopole arrangements as illustrated in Fig. 17(a), (b) and (c), respectively. All of the estimates of radiated power in Fig. 18 used modal filtering weights calculated at 50 Hz.

Observe that each of the three estimates of sound power based on the first multipole captures the peaks clearly; however, an error of a few dB is common particularly at frequencies at the higher end of the spectrum. The peak values in the sound power spectrum are contained in Table 2. Visual inspection of Fig. 18(a) and (b) shows strong similarities between the two methods when considering just the first multipole. However, Fig. 18(c) is noticeably different to the other two sub figures; the resulting decomposition based on a higher density of monopoles in the vertical plane has resulted in an estimate of radiated power which appears less accurate (based on just the first multipole). This suggests that monopoles placed in a 3D array to decompose a radiated sound field should be distributed as evenly as possible over the entire noise source.

When considering the first eight multipoles (of a total of 16) the accuracy of each of the three estimates has improved, more spectral peaks are closer to the actual values, particularly at frequencies above 500 Hz. When eight multipoles are considered the difference between the three estimates (contained in Fig. 18(a)–(c)) is smaller than when just the first multipole is considered. The denser distribution of monopoles in the vertical plane returned a similar estimate of radiated power when eight multipoles are considered. This observation suggests that as the number of multipoles used in the estimate increases, the actual spatial distribution of the monopoles becomes less important, providing the ''virtual'' monopoles used at the beginning of the

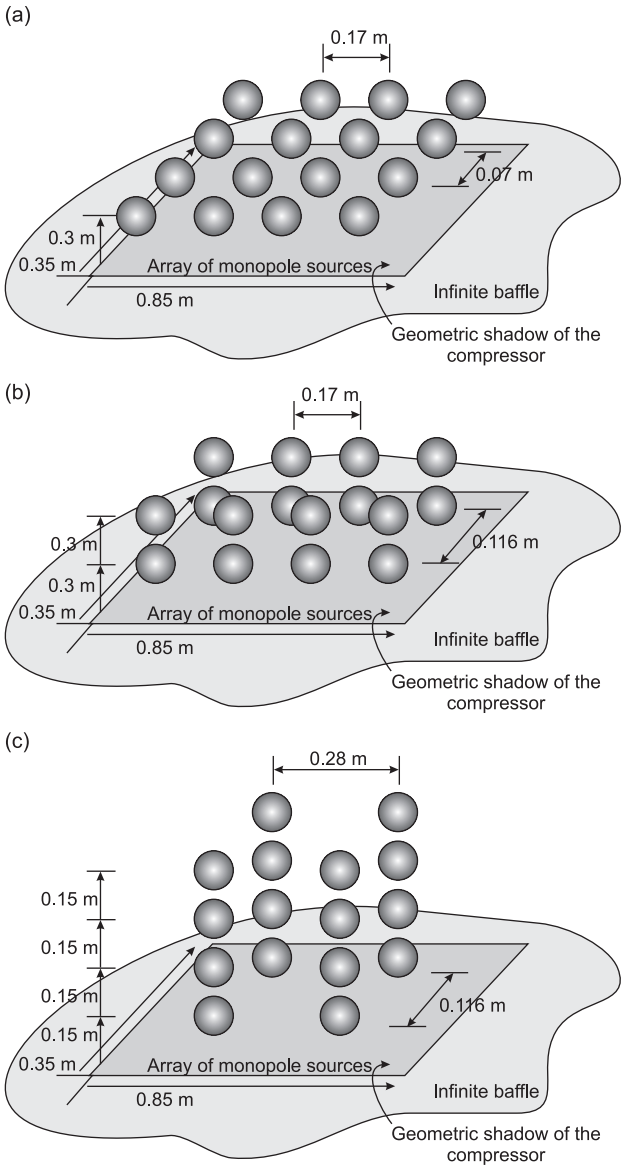

Fig. 17. Arrangements of 16 monopoles in a 3D array: (a) a single plane (1 × 16) of monopoles, (b) two planes (2 × 8) of monopoles, (c) four planes (4 × 4) of monopoles.

decomposition process are evenly distributed over the source. However, in the case of an active noise control application the number of signals used as an error signals should be minimised to reduce financial cost and computational load on the processor. Therefore it is worth trying to optimise the quality and simultaneously minimise the number of required error signals (in this case resolved multipole radiation amplitudes).

Considering again a 2D based approach for the decomposition of the 3D noise source under investigation. In the previous section eight monopoles were used in the decomposition of the radiated sound field. Now consider 16 monopoles arranged over the geometric shadow of the air compressor, as shown in Fig. 19. By using 16 monopoles in the decomposition process, 16 orthogonal multipole radiation patterns are produced; however, only a maximum of eight (the first eight based on radiation efficiency) will be considered to allow a comparison with previous sections.

Illustrated in Fig. 20 is the estimate of sound power considering the first and first eight (from a total of 16) multipole(s) based on 16 monopoles arranged as shown in Fig. 19. The values of the spectral peaks are shown

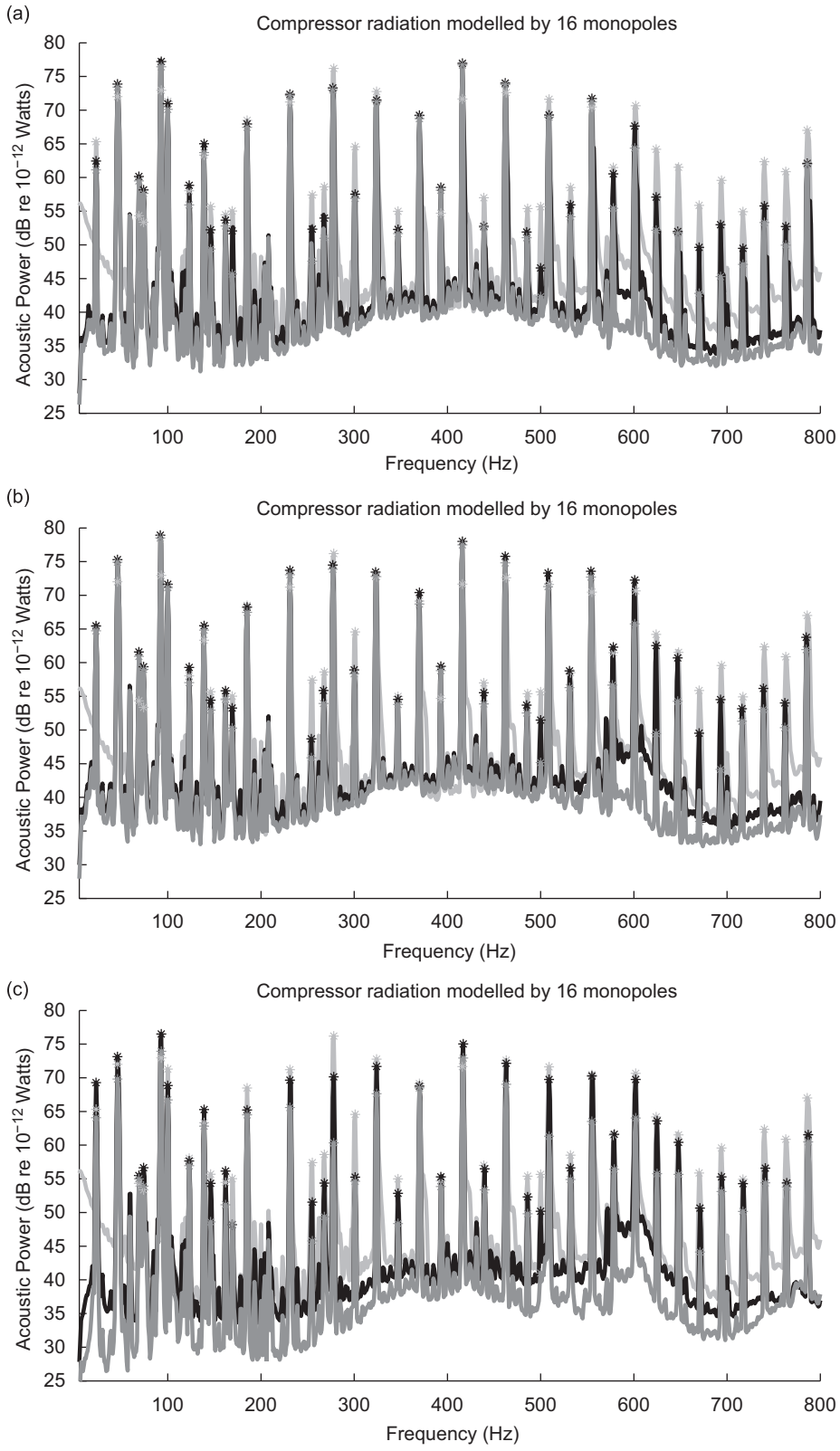

Fig. 18. Radiated power contained in the first eight multipoles based on (a) the monopole arrangement illustrated in Fig. 17(a); (b) the monopole arrangement illustrated in Fig. 17(b); and (c) the monopole arrangement illustrated in Fig. 17(c). —— One multipole estimate, —— eight multipole estimate, —— actual power.

Table 2
Sound power at peak frequencies plotted in Section 5 (peaks above 55 dB in the actual spectrum)

Peak freq. (Hz)	Actual power	Decomposition technique							
		3D multipoles						2D multipoles	
		Fig. 17(a)		Fig. 17(b)		Fig. 17(c)		Fig. 19	
		1 multi	8 multi	1 multi	8 multi	1 multi	8 multi	1 multi	8 multi
23	65.33	61.13	62.44	64.73	65.47	64.08	69.28	64.60	64.91
46	72.01	73.42	73.87	74.92	75.30	69.80	73.14	62.90	68.33
69	54.33	59.49	60.14	60.93	61.58	55.00	55.49	50.08	56.08
74	53.37	57.64	58.16	59.00	59.40	53.91	56.65	48.99	55.80
93	72.95	76.44	77.22	78.51	78.92	73.93	76.50	62.72	72.77
100	71.30	70.12	70.96	71.13	71.64	66.71	68.86	60.54	69.65
123	58.03	55.92	58.83	57.04	59.29	56.96	57.65	53.07	58.38
139	63.34	63.70	65.02	64.84	65.48	62.81	65.27	43.67	62.71
146	55.68	49.38	52.23	52.96	54.43	48.60	54.33	58.21	58.65
162	54.46	52.81	53.67	54.62	55.83	51.14	56.16	53.02	57.76
169	55.02	45.67	52.07	50.29	53.26	48.19	48.19	53.23	53.73
185	68.48	67.45	67.94	67.48	68.23	64.50	65.21	50.61	64.61
231	71.21	72.16	72.35	73.06	73.71	65.59	69.65	66.17	69.65
255	57.41	50.27	52.33	45.86	48.69	45.78	51.53	50.31	50.77
268	58.60	52.43	53.98	53.94	55.86	49.36	54.36	55.91	56.32
278	76.19	73.01	73.30	73.88	74.48	60.34	70.14	74.00	74.04
301	64.56	56.90	57.53	58.35	58.93	54.63	55.25	56.92	57.30
324	72.77	71.26	71.50	72.81	73.45	67.63	71.69	68.00	71.41
347	54.97	51.68	52.30	53.79	54.54	48.37	52.84	50.03	50.51
370	69.14	68.76	69.23	68.72	70.40	68.50	68.77	64.41	71.70
393	54.68	58.12	58.53	58.82	59.45	53.85	55.29	44.04	54.26
416	71.66	76.70	76.94	77.49	78.00	72.92	75.02	66.35	73.57
439	56.99	52.63	52.74	53.87	55.53	53.35	56.48	47.26	57.21
463	72.61	73.81	74.01	74.82	75.79	69.03	72.16	71.93	74.18
486	55.39	51.07	51.90	52.53	53.68	49.82	52.31	52.75	53.03
500	55.66	42.31	46.57	45.15	51.47	41.01	50.18	53.53	57.45
509	71.62	68.97	69.27	71.29	73.29	61.32	69.75	71.95	74.26
532	58.51	54.18	55.94	56.29	58.78	54.89	56.62	56.87	58.09
555	70.48	71.23	71.73	72.71	73.56	63.51	70.26	70.08	70.60
578	61.48	55.43	60.54	56.67	62.31	56.42	61.61	53.48	64.34
602	70.66	64.36	67.65	65.76	72.26	64.03	69.76	67.22	74.73
624	64.19	52.16	57.09	49.46	62.53	55.77	63.59	65.55	67.84
648	61.53	51.73	51.98	54.26	60.71	55.66	60.42	62.69	65.20
670	55.87	42.80	49.63	36.41	49.53	44.13	50.66	53.39	54.79
694	59.57	45.27	53.00	44.15	54.50	53.11	55.29	55.18	56.97
717	54.93	47.11	49.48	51.31	53.16	50.15	54.28	51.54	53.04
740	62.35	53.33	55.78	53.06	56.17	54.41	56.58	54.73	55.33
763	60.86	49.96	52.73	50.34	54.02	53.80	54.39	54.71	58.78
786	67.00	61.95	62.10	61.93	63.77	60.47	61.55	66.11	66.78

Peak data are in dB re 10^{-12} W.

in Table 2. The decomposition uses modal filtering weights calculated at 50 Hz. The 2D decomposition used here has resulted in a practical estimation of radiated power over a majority of the frequency range 5–800 Hz. In comparison to the similar estimate of radiated power in Fig. 14, the use of additional monopoles (when just the first shape is considered) at the modelling stage of the decomposition seems to have provided little benefit. However, when the estimate of sound power from the first eight multipoles (based on 16 monopoles), as plotted in Fig. 20, is compared to that generated from eight multipoles (based on eight monopoles) in Fig. 14 (and also comparing the values in Tables 1 and 2), the accuracy of the estimate over the entire frequency range has improved—though not significantly.

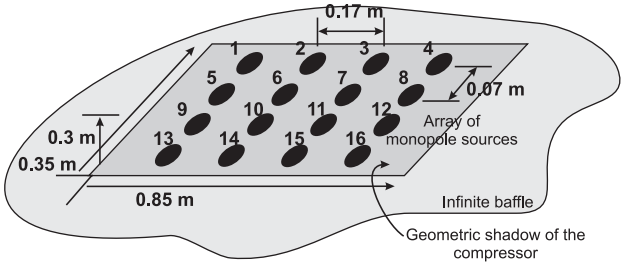

Fig. 19. The 2D arrangement for 16 monopoles.

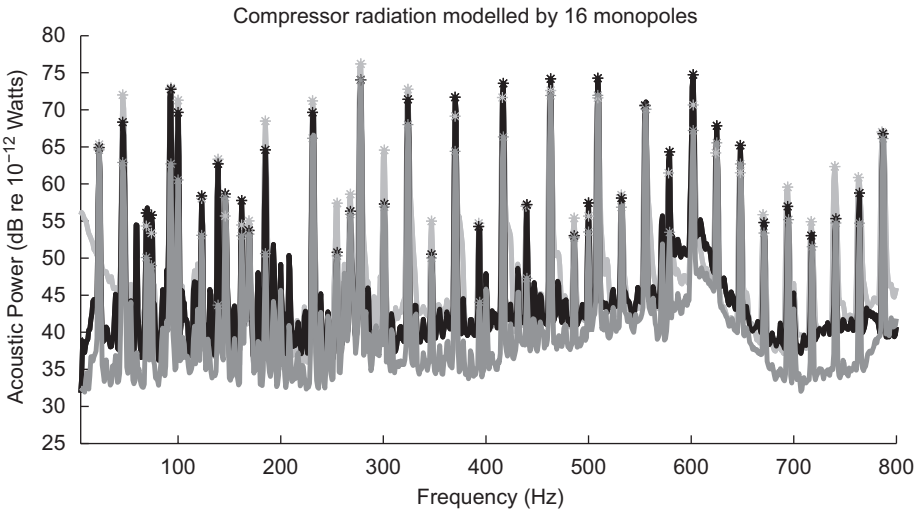

Fig. 20. Radiated power decomposition using the monopole arrangement illustrated in Fig. 19. ——— One multipole estimate, ——— eight multipole estimate, ——— actual power.

6. Conclusions

This work has examined the problem of developing and practically implementing a generalised sensing system which is capable of measuring the global sound radiation (sound power) from a 3D noise source.

The heart of the strategy is to decompose radiation from any sound field into a set of orthogonal acoustic multipoles which are combinations of a 3D array of in- and out-of-phase "virtual" monopoles, which are placed "in concept" within/on the noise source. The work postulates that the total sound radiation from any noise source can be described by weighted contributions of orthogonal radiation patterns, termed 3D multipoles. This idea is analogous to total vibration being described by the sum of the amplitudes of each vibration mode. As the orthogonal contributors to sound power are described by an array of acoustic monopoles, in the acoustic domain (no structural information is required, just a set of sound pressure measurements), the decomposition is applicable to any noise source. Hence the sensing approach earns the description of a generalised sensing strategy.

Previous work in the area of global sound power sensing for 3D sources has tended to take a vibration-centric approach to sensing system design. The requirement of detailed structural knowledge inherent in these approaches has limited the prospect of moving the sensing system from simulation or small-scale laboratory implementation to more practical problems. The approach presented here is acoustic-centric, overcoming the need of detailed structural knowledge, opening application to a wider range of 3D noise sources.

We have presented experimental results which compare the sum of different numbers of orthogonal contributors to sound power to the actual sound power spectrum for an air compressor (which is not a structural noise source). An air compressor presents several problems to traditional sensing system design

strategies, e.g. the actual path of radiation is difficult to determine, where should the designer place structural sensors on the source, etc. The three decomposition methods considered gave an accurate estimate of a practical nature of the global error (sound power), at least over a small frequency range. Thus the output signals from the modal filtering process are a set of signals amendable to any particular type of control approach (e.g. feedforward or feedback). Even the two decompositions which postulated a 2D noise source produced a useful estimate of the global error criterion. While the 2D decompositions yielded an estimate of radiated power close to the actual level, the same result may not occur if the noise source is large in comparison to wavelength, particularly the height of the source.

In the experimental analysis we analysed the effect on the number of monopoles used in the decomposition and their distribution in the array. It was difficult to distinguish between the estimates of radiated power for eight or more multipoles. Results indicated that the spatial resolution of the monopoles used in the decomposition had a secondary effect on accuracy, in comparison to the number of considered constituents (as long as the "virtual" monopoles are evenly distributed over the noise source which is under consideration).

Acknowledgements

The authors wish to thank George Osborne and George Vokalek for their technical support in completion of the microphone arrays and the modal filtering system, respectively. Some of this work was completed as part of the first author's Ph.D. studies at the University of Adelaide. The first author gratefully acknowledges support towards this work by the Japan Society for the Promotion of Science.

References

[1] W.L. Meyer, W.A. Bell, B.T. Zinn, M.P. Stallybrass, Boundary integral solutions of three dimensional acoustic problems, *Journal of Sound and Vibration* 59 (2) (1978) 245–262.
[2] L.B. Felsen, J.M. Ho, I.T. Lu, Three-dimensional Green's function for fluid-loaded thin elastic cylindrical shell: formulation and solution, *Journal of the Acoustical Society of America* 87 (2) (1990) 543–553.
[3] D.E. Montgomery, R.L. West, R.A. Burdisso, Acoustic radiation prediction of a compressor housing from three-dimensional experimental spatial dynamics modeling, *Applied Acoustics* 47 (2) (1996) 165–185.
[4] D. Giljohann, M. Bittner, The three-dimensional DtN finite element method for radiation problems of the Helmholtz equation, *Journal of Sound and Vibration* 212 (3) (1998) 383–394.
[5] D.S. Burnett, A three-dimensional acoustic infinite element based on a prolate spheroidal multipole expansion, *Journal of the Acoustical Society of America* 96 (5) (1994) 2798–2816.
[6] J.A. Giordano, K.A. Cunefare, G.H. Koopmann, An experiment of optimization of active noise control on a three-dimensional extended radiator, *ASME Journal of Vibration and Acoustics* 115 (1993) 53–58.
[7] C.H. Hansen, S.D. Snyder, *Active Control of Noise and Vibration*, E & FN Spon, London, 1997.
[8] D.A. Bies, C.H. Hansen, *Engineering Noise Control*, second ed., E & FN Spon, London, 1997.
[9] D.J. Mead, *Passive Vibration Control*, Wiley, New York, 1998.
[10] K.A. Cunefare, G.H. Koopmann, A boundary element approach to optimization of active noise control sources on three-dimensional structures, *ASME Journal of Vibration and Acoustics* 113 (1) (1991) 387–394.
[11] T.D. Gordy, Audible noise of power transformers, *Transactions of the American Institute of Electrical Engineers* 69 (1950) 45–53.
[12] W.B. Conover, Fighting noise with noise, *Noise Control Engineering Journal* 2 (1956) 78–82, 92.
[13] A. Sakuta, J. Kowalewski, M. Colbert, Assessment technique for controlliong transformer noise, *Proceedings of InterNoise 92, Toronto*, 1992, pp. 783–786.
[14] N. Hesselmann, Investigation of noise reduction on a 100 KVA transformer tank by means of active methods, *Applied Acoustics* 11 (1) (1978) 27–34.
[15] O.L. Angevine, Active acoustic attenuation of electric transformer noise, *Proceedings of InterNoise 81*, 1981, pp. 303–306.
[16] O.L. Angevine, S.E. Wright, Active cancellation of the hum of a simulated electric transformer, *Proceedings of InterNoise 90*, 1990, pp. 789–792.
[17] X. Li, X. Qiu, R. Gu, R. Köehler, C.H. Hansen, Active control of large electrical transformer noise using near-field error sensing, *Proceedings of the AAS Conference*, 1999, pp. 141–148.
[18] X. Li, Physical Systems for the Active Control of Transformer Noise, PhD Thesis, The University of Adelaide, 2000.
[19] L. Meirovitch, H. Öz, Modal-space control of large flexible spacecraft possessing ignorable coordinates, *AIAA Journal of Guidance, Control and Dynamics* 3 (6) (1980) 569–577.
[20] L. Meirovitch, H. Baruh, Control of self-adjoint distributed-parameter systems, *AIAA Journal* 5 (1) (1982) 60–66.
[21] L. Meirovitch, H. Baruh, The implementation of modal filters for control of structures, *AIAA Journal of Guidance Control and Dynamics* 8 (6) (1985) 707–719.

[22] C.-K. Lee, F.C. Moon, Modal sensors/actuators, *Journal of Applied Mechanics* 57 (1990) 434–441.
[23] D.R. Morgan, An adaptive modal-based active control system, *Journal of the Acoustical Society of America* 89 (1) (1991) 248–256.
[24] S.A. Lane, R.L. Clark, S.C. Southward, Active control of low frequency modes in an aircraft fuselage using spatially weighted arrays, *ASME Journal of Vibration and Acoustics* 122 (2000) 227–234.
[25] S.D. Snyder, N.C. Burgan, N. Tanaka, An acoustic-based modal filtering approach to sensing system design for active control of structural acoustic radiation: theoretical development, *Mechanical Systems and Signal Processing* 16 (1) (2002) 123–139.
[26] N.C. Burgan, S.D. Snyder, N. Tanaka, A.C. Zander, A generalised approach to modal filtering for active noise control, part I: vibration sensing, *IEEE Sensors Journal* 2 (6) (2002) 577–589.
[27] S.G. Hill, S. D Snyder, B.S. Cazzolato, N. Tanaka, R. Fukuda, A generalised approach to modal filtering for active noise control, part II: acoustic sensing, *IEEE Sensors* 2 (6) (2002) 590–596.
[28] G.V. Borgiotti, The power radiated by a vibrating body in an acoustic fluid and its determination from boundary measurements, *Journal of the Acoustical Society of America* 88 (4) (1990) 1884–1893.
[29] D.M. Photiadis, The relationship of singular value decomposition to wave-vector filtering in sound radiation problems, *Journal of the Acoustical Society of America* 88 (2) (1990) 1152–1159.
[30] A. Sarkissian, Acoustic radiation from finite structures, *Journal of the Acoustical Society of America* 90 (1) (1991) 574–578.
[31] K.A. Cunefare, The minimum multimodal radiation efficiency of baffled finite beams, *Journal of the Acoustical Society of America* 90 (5) (1991) 2521–2529.
[32] W.T. Baumann, W.R. Saunders, H.H. Robertshaw, Active suppression of acoustic radiation from impulsively excited structures, *Journal of the Acoustical Society of America* 90 (6) (1991) 3202–3208.
[33] W.T. Baumann, F.-S. Ho, H.H. Robertshaw, Active structural acoustic control of broadband disturbances, *Journal of the Acoustical Society of America* 92 (4) (1992) 1998–2005.
[34] K. Naghshineh, G.H. Koopmann, A design method for achieving weak radiator structures using active vibration control, *Journal of the Acoustical Society of America* 92 (2) (1992) 856–870.
[35] K. Naghshineh, G.H. Koopmann, A.D. Belegundu, Material tailoring of structures to achieve a minimum radiation condition, *Journal of the Acoustical Society of America* 92 (2) (1992) 841–855.
[36] S.D. Snyder, N. Tanaka, On feedforward active control of sound and vibration using vibration error signals, *Journal of the Acoustical Society of America* 94 (4) (1993) 2181–2193.
[37] S.J. Elliott, M.E. Johnson, Radiation modes and the active control of sound power, *Journal of the Acoustical Society of America* 94 (4) (1993) 2194–2204.
[38] K. Naghshineh, G.H. Koopmann, Active control of sound power using acoustic basis functions as surface velocity filters, *Journal of the Acoustical Society of America* 93 (5) (1993) 2740–2752.
[39] K.A. Cunefare, M.N. Currey, On the exterior acoustic radiation modes of structures, *Journal of the Acoustical Society of America* 96 (4) (1994) 2302–2312.
[40] A. Berry, Advanced sensing strategies for the active control of vibration and structural radiation, *Noise Control Engineering Journal* 49 (1) (2001) 54–65.
[41] A.P. Berkhoff, Broadband radiation modes: estimation and active control, *Journal of the Acoustical Society of America* 111 (3) (2002) 1295–1305.
[42] K.A. Cunefare, M.N. Currey, M.E. Johnson, S.J. Elliott, The radiation efficiency grouping of free-space acoustic radiation modes, *Journal of the Acoustical Society of America* 109 (1) (2001) 203–215.
[43] G.H. Koopmann, L. Song, J.B. Fahnline, A method for computing acoustic fields based on the principle of wave superposition, *Journal of the Acoustical Society of America* 86 (6) (1989) 2433–2438.
[44] S.A. Yang, An integral equation approach to three-dimensional acoustic radiation and scattering problems, *Journal of the Acoustical Society of America* 116 (3) (2004) 1372–1380.
[45] K.A. Cunefare, G.H. Koopmann, Global optimum active noise control: surface and far-field effects, *Journal of the Acoustical Society of America* 90 (1) (1991) 365–373.
[46] K.A. Cunefare, G.H. Koopmann, Acoustic design sensitivity for structural radiators, *ASME Journal of Vibration and Acoustics* 114 (1) (1992) 178–186.
[47] S.D. Snyder, Microprocessors for active control: bigger is not always enough, *Noise Control Engineering* 49 (2001) 21–29.
[48] S.G. Hill, S.D. Snyder, Acoustic based modal filtering of orthogonal radiating functions for active noise control: part I theory and simulation, *Mechanical Systems and Signal Processing* 21 (4) (2007) 1815–1838.
[49] S.G. Hill, N. Tanaka, S.D. Snyder, Acoustic based modal filtering of orthogonal radiating functions for active noise control: part II implementation, *Mechanical Systems and Signal Processing* 21 (5) (2007) 1937–1952.
[50] B.D.O. Anderson, J.B. Moore, *Optimal Control, Linear Quadratic Methods*, Prentice-Hall, Englewood Cliffs, NJ, 1990.
[51] D.C. Baumann, R.A. Greiner, Number of error microphones for multi-modal cancellation, *Proceedings of InterNoise 92*, 1992, pp. 345–348.
[52] N.K. Gupta, Frequency-weighted loop functions: extensions of linear-quadratic-gaussian design methods, *Journal of Guidance and Control* 3 (6) (1980) 529–535.
[53] U. Ingard, On the reflection of a spherical sound wave from a infinite plane, *Journal of the Acoustical Society of America* 23 (3) (1951) 329–335.
[54] U. Ingard, L. Lamb Jr., Effect of a reflecting plane on the power output of sound sources, *Journal of the Acoustical Society of America* 29 (6) (1957) 743–744.
[55] H. Levine, A note on sound radiation from distributed sources, *Journal of Sound and Vibration* 68 (2) (1980) 203–207.

[56] H. Levine, Output of acoustical sources, *Journal of the Acoustical Society of America* 67 (6) (1980) 1935–1946.
[57] H. Levine, On source radiation, *Journal of the Acoustical Society of America* 68 (4) (1980) 1199–1205.
[58] P.A. Nelson, S.J. Elliott, The minimum power output of a pair of free field monopole sources, *Journal of Sound and Vibration* 105 (1) (1986) 173–178.
[59] P.A. Nelson, A.R.D. Curtis, S.J. Elliott, A.J. Bullmore, The minimum power output of free field point sources and the active control of sound, *Journal of Sound and Vibration* 116 (3) (1987) 397–414.
[60] H.F. Harmuth, *Transmission of Information by Orthogonal Functions*, second ed., Springer, Berlin, 1972.
[61] R.J. Pinnington, D.C.R. Pearce, Multipole expansion of the vibration transmission between a source and receiver, *Journal of Sound and Vibration* 142 (3) (1990) 461–479.
[62] S.D. Snyder, C.H. Hansen, Mechanisms of active noise control by vibration sources, *Journal of Sound and Vibration* 147 (3) (1991) 519–525.
[63] J. Pan, S.D. Snyder, C.H. Hansen, C.R. Fuller, Active control of far-field sound radiated by a rectangular panel—a general analysis, *Journal of the Acoustical Society of America* 91 (4) (1992) 2056–2066.
[64] S.D. Snyder, N. Tanaka, To absorb or not to absorb: control source power output in active noise control systems, *Journal of the Acoustical Society of America* 94 (1) (1993) 185–195.
[65] P.A. Nelson, S.H. Yoon, Estimation of acoustic source strength by inverse methods: part I, conditioning of the inverse problem, *Journal of Sound and Vibration* 233 (4) (2000) 643–668.
[66] S.H. Yoon, P.A. Nelson, Estimation of acoustic source strength by inverse methods: part II, experimental investigation of methods for choosing regularization parameters, *Journal of Sound and Vibration* 233 (4) (2000) 699–705.
[67] A.P. Berkhoff, Sensor scheme design for active structural acoustic control, *Journal of the Acoustical Society of America* 108 (3) (2000) 1037–1045.
[68] Y. Kim, P.A. Nelson, Spatial resolution limits of the reconstruction of acoustic source strength by inverse methods, *Journal of Sound and Vibration* 265 (3) (2003) 583–608.
[69] A.N. Thite, D.J. Thompson, The quantification of structure-borne transmission paths by inverse methods. Part 2: use of regularization techniques, *Journal of Sound and Vibration* 264 (2) (2003) 433–451.
[70] C.H. Hansen, Active noise control—from laboratory to industrial implementation, *Proceedings of Noise-Con '97*, 1997, pp. 3–38.
[71] S.D. Snyder, *Active Noise Control Primer*, Springer, Berlin, 2000.
[72] C.H. Hansen, *Understanding Active Noise Cancellation*, Spon Press, London, 2001.
[73] S.D. Snyder, S.G. Hill, N.C. Burgan, N. Tanaka, B.S. Cazzalato, Acoustic-centric modal filter design for active noise control, *Control Engineering Practice* 12 (8) (2004) 1055–1064.